國 立 交 通 大 學

電信工程學系

博 士 論 文

超密波長分工及次載波有線電視系統的
基本限制

Fundamental Transmission Limitations on both
Ultra-Dense WDM and
Subcarrier Multiplexed CATV Systems
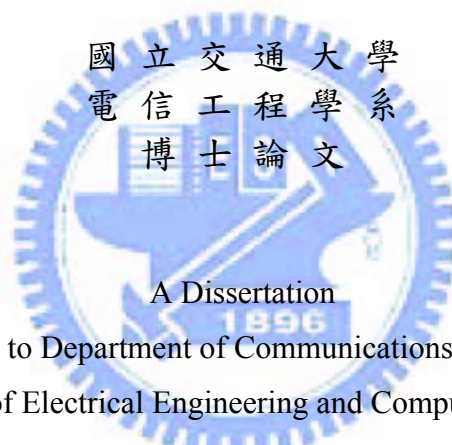
研究生：吳明佳

指導教授：尉應時

中 華 民 國 九十三 年 七 月

超密波長分工及次載波有線電視系統的基本限制
Fundamental Transmission Limitations on both Ultra-Dense WDM and Subcarrier Multiplexed CATV Systems

研 究 生：吳明佳　　　　Student：Ming-Chia Wu

指導教授：尉應時　　　　Advisor：Winston I. Way

國 立 交 通 大 學
電 信 工 程 學 系
博 士 論 文

A Dissertation

Submitted to Department of Communications Engineering

College of Electrical Engineering and Computer Science

National Chiao Tung University

in partial Fulfillment of the Requirements

for the Degree of

Doctor of Philosophy

in

Communications Engineering

July 2004

Hsinchu, Taiwan, Republic of China

中華民國九十三年七月

超密波長分工及次載波有線電視系統的基本限制

學生：吳明佳　　　　　　指導教授：尉應時

國立交通大學電信工程學系

摘　　　要

本論文研究超密波長分工系統及次載波有線電視系統的基本限制．　主要分為四個部份：在第一部分中，我們分析了 2.5 及 10 Gb/s 的超密波長分工系統在不同單模光纖中的傳輸限制並分析了週期性放大的系統在 C 波帶的各項基本限制及最佳色散補償比例．　第二部分，我們發現在 1550nm 外調式類比有線電視系統中，自發性及外加相位調變必須同時考慮才能精準地預測二階拍差，特別是當外加相位調變的調變深度或頻率高的時侯．這個結果對長距離 1550nm 外調式光發射機的設計有很重要的影響．　第三部分，我們證明了用多個 CW 載波來模擬測試 M-QAM 次載波有線電視系統的準確度是在量測誤差的範圍內．　最後，我們架設了世界第一個類比的光纖循環迴圈並創造了 78 個頻道 64-QAM 1550nm 次載波系統的最長傳輸記錄-740km．

Fundamental Transmission Limitations on both Ultra-Dense WDM and Subcarrier Multiplexed CATV Systems

Student：Ming-Chia Wu   Advisors：Dr.Winston I. Way

Department of Communications Engineering
National Chiao Tung University

ABSTRACT

This thesis investigates fiber nonlinearity limitation in both ultra dense wavelength division multiplexing (U-DWDM) digital systems and subcarrier multiplexing analog lightwave transmission systems.　The main research results are organized into four parts.

First of all, transmission performance of ultra-dense 2.5 and 10 Gbps NRZ IM/DD wavelength division multiplexing systems in various single-mode fibers is investigated. Fundamental limiting factors and their remedies by using optimum dispersion compensation for periodically amplified systems in C-band are presented.

Second, we found that the combined effects of self- and external-phase modulations must be considered in order to precisely predict the CSO distortions in a long-distance 1550 nm externally-modulated AM-CATV system, especially when the applied phase modulation index and modulating tone frequency to the integrated phase modulator are high.　This result has important implications to the optimum design of 1550 nm transmitter for long-distance AM- and QAM-CATV systems.

Third, the validity of using multiple CW tones as the signal source to test the linearity of a multichannel M-ary quadrature-amplitude-modulation (M-QAM) subcarrier multiplexed (SCM) lightwave system was investigated.　We consider the following representative optical fiber system nonlinearities: (1) laser clipping, and (2) the combined effect of laser frequency chirp and fiber dispersion.　The results show that, if all orders of nonlinear distortions (NLDs) in a signal bandwidth are included in the total NLD power, the error caused by replacing M-QAM signals with CW tones can be within measurement uncertainty.

Finally, a long-distance 1550 nm subcarrier multiplexed lightwave trunk system which transported 78 channels of 64-QAM signals was demonstrated in a recirculating loop experiment.　Each channel can achieve a carrier-to-(noise + nonlinear distortion) ratio of 30 dB after 740 km transmission through conventional single-mode fiber without dispersion compensation.

誌　　　　謝

　　時光飛逝，我在交大已過了十幾個年頭，這一路走來要感謝的人很多，首先感謝系上的師長及口試委員給我很多意見及指導，也非常感謝我的老師尉應時及其家人，在國內外都關心我的生活，讓我有機會學習社會的經驗·感謝實驗室的學長及學弟帶給我許多歡樂及幫助，在此也感謝系上行政人員給我相當大幫助· 最後，將此論文獻給我的家人，因為有你們的支持才能讓我無後顧之憂的完成學業·

Index

Table Index

Figure Index

1. Introduction

This thesis investigates fundamental transmission limitations in both ultra dense wavelength division multiplexing (U-DWDM) digital systems and subcarrier multiplexing lightwave systems. The main research results are organized in four parts as follows.

First of all, transmission performance of ultra-dense 2.5 and 10 Gbps NRZ IM/DD wavelength division multiplexing systems in various single-mode fibers is investigated. Fundamental limiting factors and their remedies by using optimum dispersion compensation for periodically amplified systems in C-band are presented.

In order to increase the transmission capacity of a DWDM optical system, one can either increase the transmission data rate per wavelength, or increase the number of wavelengths while keeping proper transmission granularity. The first approach can be illustrated by the recent increase in data rate per wavelength from 2.5 Gbps to 10 and 40 Gbps. The second approach is to significantly increase the number of wavelengths in a fixed optical spectrum (e.g., C-band) by decreasing the spacing between neighboring wavelengths. By using this approach, capacity increase can be achieved without resorting to high-speed (e.g., > 40 Gbps) electronics, while keeping compatibility with existing 2.5/10 Gbps SONET/SDH equipment. Along this line, the focus of this paper is on ultra-dense wavelength division multiplexing (U-DWDM) transmission systems. Examples of U-DWDM systems include 25 GHz-spaced 10 Gbps and 6.25 GHz-spaced 2.5 Gbps transmission systems.

It should be noted that, even though a few U-DWDM system experiments have been carried out recently [1-5], the fundamental limiting factors and their remedies in such systems remain unclear. It is obvious that there are different transmission issues to be dealt with in the above-mentioned two distinct approaches. When the transmitting data rate is higher than 40 Gbps, severe chromatic dispersion and polarization mode dispersion problems will have to be resolved even before dealing with optical nononlinearity-induced penalties. On the other hand, U-DWDM systems intuitively should have optical nonlinearity-induced system limitations such as four-wave mixing (FWM) and cross-phase modulation (XPM) penalties. The first part of this thesis considers various nonlinear distortions/interferences to determine the fiber nonlinearity limited maximum transmission distances in U-DWDM systems. Optimum launched power and dispersion compensation ratio (DCR), and the dominant optical nonlinearities in different systems are

also discussed.

In Section 2.1, we provide an overview of the main nonlinear distortions/interferences in U-DWDM systems. In Section 2.2, we analytically calculate and numerically simulate the capacity and distance limitations of U-DWDM systems. Discussions and conclusions are provided in Sections 2.3 and 2.4, respectively.

Second, we found that the combined effects of self- and external-phase modulations must be considered in order to precisely predict the CSO distortions in a long-distance 1550 nm externally-modulated AM-CATV system, especially when the applied phase modulation index and modulating tone frequency to the integrated phase modulator are high. This result has important implications to the optimum design of 1550 nm transmitter for long-distance AM- and QAM-CATV systems.

Recently, there has been intense interests in long-distance 1550 nm external-modulation AM-CATV systems based on conventional single-mode fibers [6-13]. When the optical power launched into these long-distance systems is below the stimulated Brillouin scattering (SBS) threshold, it has been found that the transmission distance is mainly limited by the fiber dispersion-induced composite second order (CSO) distortions. These CSO distortions in turn were believed to be caused by self-phase modulation (SPM) [8-10], and by the residual intensity modulation from an imperfect phase modulator [11]. However, analyses developed for either of the above mechanisms were not accurate in predicting the resultant CSO values in long-distance AM-CATV transmission systems [10-12].

It is noted that all commercially available 1550 nm CATV transmitters have an integrated phase modulator and a Mach-Zehnder interferometer (MZI) modulator. In order to increase the SBS threshold, a ~2 GHz tone (or a few tones > ~2GHz) is usually applied to the phase modulator, and a high SBS threshold can be obtained by using a high phase modulation (PM) index (β) [13]. However, the resultant high launched optical power into the system can unavoidably increase the SPM effects. In addition, when the applied PM index β or the PM modulating tone frequency are high, or when the transmission distance is long, both SPM and external phase modulation (EPM) can be mixed with intensity modulation in a nonlinear dispersive optical fiber system. The resultant CSO distortions due to their combined effects, however, have not yet been thoroughly investigated. Section 3 of this thesis presents both experimental and numerical results on the above subject.

Third, the validity of using multiple CW tones as the signal source to test the linearity of a multichannel M-ary quadrature-amplitude-modulation (M-QAM) subcarrier multiplexed (SCM) lightwave system was investigated.　We consider the following representative optical fiber system nonlinearities: (1) laser clipping, and (2) the combined effect of laser frequency chirp and fiber dispersion.　The results show that, if all orders of nonlinear distortions (NLDs) in a signal bandwidth are included in the total NLD power, the error caused by replacing M-QAM signals with CW tones can be within measurement uncertainty.

It is believed that SCM lightwave systems can be used to transport multichannel M-QAM signals to provide broadband digital services such as Internet access, digital video, IP telephony, etc. [14,15].　In the past, the linearity characteristics of such systems were investigated by using multiple CW tones [16-18], mainly because of the practical difficulty in generating multiple distinct M-QAM channels.　However, the spectral distributions of nonlinear distortions (NLDs) caused by multiple CW tones and multiple wideband M-QAM signals are quite different.　In the former case, NLDs consist of various distinct beats such as composite second orders (CSOs) and composite triple beats (CTB's).　In the latter case, NLDs are spread over several channels and are like white noise.　Fig.1 (a) and (b) illustrate the spectra of the two cases.　To our knowledge, there is no report discussing the validity of using CW tones to replace the actual M-QAM signals.　In section 4 of this thesis, we study this validity by performing spectral analysis, numerical simulation and experimental verification.　We chose two representative optical fiber nonlinearities in SCM lightwave systems to study: (1) laser clipping, and (2) the combined effect of laser chirping and optical fiber dispersion.
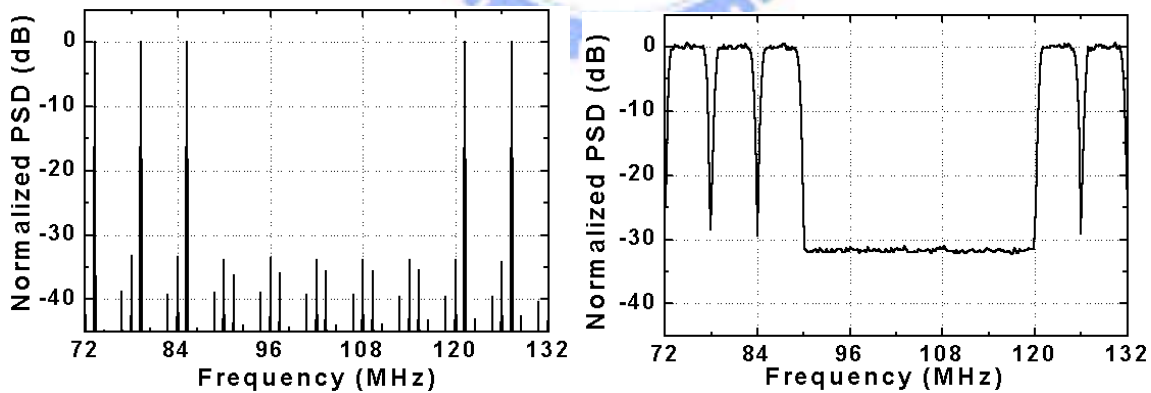
Fig. 1 Illustrations of　typical　NLDs generated from (a) CW tones and (b) QAM.　Signal level were normalized to 0 dB for comparison.

Finally, a long-distance 1550 nm subcarrier multiplexed lightwave trunk system which transported 78 channels of 64-QAM signals was demonstrated in a recirculating loop experiment.　Each channel can

achieve a carrier-to-(noise + nonlinear distortion) ratio of 30 dB after 740 km transmission through conventional single-mode fiber without dispersion compensation.

A subcarrier multiplexed (SCM) lightwave system transporting multi-channel M-ary quadrature-amplitude-modulation (M-QAM) signals can have transmission features such as high system capacity and long transmission distance [19-20]. This is due to the fact that the carrier-to-noise ratio (CNR) and carrier-to-nonlinear distortion ratio (CNLD) requirements of M-QAM signals are lower than those of AM-VSB signals. In addition, M-QAM signals have a high spectral efficiency, which makes multi-gigabit/sec data transmission feasible when using conventional CATV optical transceivers. Therefore, multi-channel M-QAM SCM trunk systems have a great potential to be used for interconnecting CATV headends and delivering various digital communication services.

It was found that the fundamental M-QAM system capacity of either a laser diode- or a linearized external modulator-based transmitter could be as high as tens of gigabit/sec [22, 23]. However, the transmission distances of all reported M-QAM SCM systems are still rather limited. In section 5 of this thesis, we experimentally demonstrated that the transmission distance of an M-QAM external modulation SCM system carrying an equivalent data capacity of 2.34 Gb/s could exceed 740 km. In addition, for the first time, an optical fiber recirculating loop was implemented in an SCM system experiment.

2. Fiber Nonlinearity Limitations in Ultra-Dense WDM Systems

2.1. Fundamental Limiting Factors in U-DWDM Systems

The three fundamental limiting factors in U-DWDM systems include (1) various random noise terms, (2) fiber chromatic dispersion-induced inter-symbol interference (ISI), and (3) optical-nonlinearity-induced distortion and interference. All three factors are common to conventional DWDM systems, although the third factor can be unique in the case of extremely close channel spacing.

We assume a multi-segmented, optically amplified U-DWDM system as shown in Fig. 2(a) to derive the general forms of fiber nonlinearity induced interferences/distortions. The transmitter side contains M external-modulated light sources at wavelength λ_i, where i=1, 2,..., M. The M wavelengths are Non-Return to ZERO (NRZ) modulated with independent data pattern and are multiplexed and demultiplexed by either a pair of ideal multiplexer and demultiplexer, or by a pair of broadband couplers

(with an ideal filter in each receiver).   A tunable post dispersion compensator (PDC), which can be tuned up to –2000 ps/nm, is located right before each optical receiver to optimize the received signal performance of each individual channel.   The nth segment contains a span $L^{(n)}$ of fiber and an erbium-doped optical amplifier with a noise figure of 5dB and a power gain $g^{(n)} = \exp(\alpha^{(n)} L^{(n)})$ to compensate the fiber loss.   The fiber can be either SMF, or NZDSF, or dispersion compensation fibers (DCFs) used for broadband dispersion compensation.   Fiber parameters assumed for analysis and numerical simulations throughout this paper are summarized in Table 1.   When dispersion compensation fibers are used in a transmission link, their additional loss must be compensated by additional stages of optical amplifiers.   In this case, we use a system configuration shown in Fig.2(b), which can be considered a special case of Fig.2(a).   Note that in Fig. 2(b), each amplifier stage comprises a span of SMF (or NZDSF), an optical amplifier to compensate the fiber loss, a span of DCF whose span length is determined by the designed DCR, and another optical amplifier to compensate for the DCF loss.   Therefore, it is equivalent to having a total of 2N stages in the general system model shown in Fig. 2(a).   We will use this periodically amplified and dispersion-compensated system model to analyze the optimum design of U-DWDM systems in Section III.

	SMF	NZDSF	DCF
Chromatic Dispersion, D(ps/nm/km)	16-18	2-6	-85
Effective core area, A_{eff}(μm^2)	85	72	21
Nonlinear refractive index, n_2(m^2/W)	2.5×10^{-20}	2.5×10^{-20}	2.5×10^{-20}
Attenuation, α (dB/km)	0.2	0.2	0.4
Dispersion Slope @1545nm (ps/nm^2/km)	0.058	0.11	-

Table 1 Fiber parameter assumptions
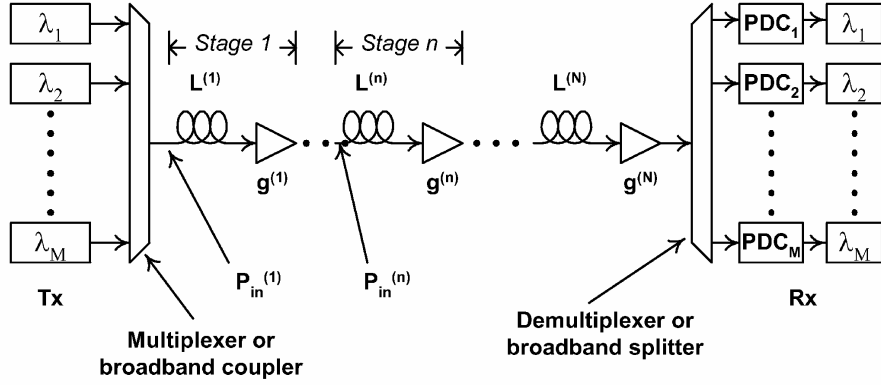
(a)
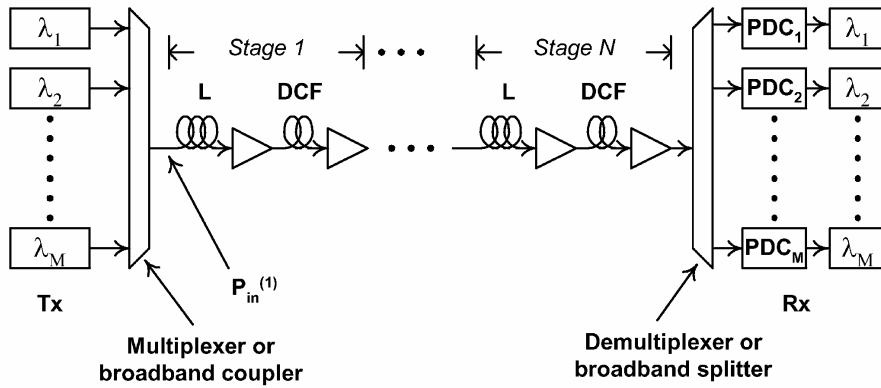
(b)

Fig. 2 (a) A general U-DWDM system model; (b) A periodically amplified U-DWDM system
model with post dispersion compensation in every amplifier stage.

Throughout this paper, we will use Q^2 = 15.6 dB (which gives $BER = 10^{-9}$ under the assumption of Gaussian distributed noise) as the minimum system performance requirement. Q^2 follows the conventional Q^2 definition and is given by

$$Q^2(dB) = 20\log_{10}\left(\frac{m_1 - m_0}{\sigma_1 + \sigma_0}\right) \tag{1}$$

where m_i and σ_i are the mean and standard deviation values for mark (i=1) and space (i=0), respectively. This system requirement assures error-free transmission when typical forward error correction (FEC)

encoders/decoders are added. It should be noted that although many published analytical results showed that nonlinear distortions or interference are usually non-Gaussian distributed, they did show that under small optical nonlinearity penalties, Gaussian approximation can serve as an upper bound and can be viewed as a good approximation [24-25]. As will be seen later in our analysis, fiber nonlinearity-induced distortions/interference is assumed to be of the same order of magnitude as amplified spontaneous emission (ASE) noise, and at $Q^2 = 15.6$ dB it can be considered small enough to be approximated as random noise just as ASE noise. Note that optical-signal-to-noise ratio (OSNR) [26-27] is not used as a performance index in our study. This is because XPM and self-phase-modulation (SPM) are not measurable in optical domain unless they are converted to electrical signal at a photo-detector.

The nonlinear interferences/distortions under consideration typically occur at mark, and thus $\sigma_1^2 >> \sigma_0^2$. The standard deviation σ_1 in (1) is modeled as

$$\sigma_1^2 = \sigma_{ASE,1}^2 + \sigma_{NL,1}^2 \tag{2}$$

where $\sigma_{ASE,1}^2$ is the noise variance due to optical amplifiers, and is dominated by signal-spontaneous emission beat noise at the presence of mark. $\sigma_{NL,1}^2 = \sigma_{FWM,1}^2 + \sigma_{XPM,1}^2 + \sigma_{SPM,1}^2$ is the interference/distortion variance due to fiber nonlinearities, including FWM, XPM and SPM. Note that although SPM induces deterministic waveform distortion, we approximate it as a normal variance term $\sigma_{SPM,1}^2$ because (1) we want to compare the effect of SPM with that of FWM and XPM across various DCR, distances, fibers, and data rates by using the same parameter, and (2) in cases where SPM distortion has the same order of magnitude as FWM/XPM interference, it is difficult to separate deterministic distortion from random interference in numerical simulations. The range of validity for this approximation will be shown in Fig.3.
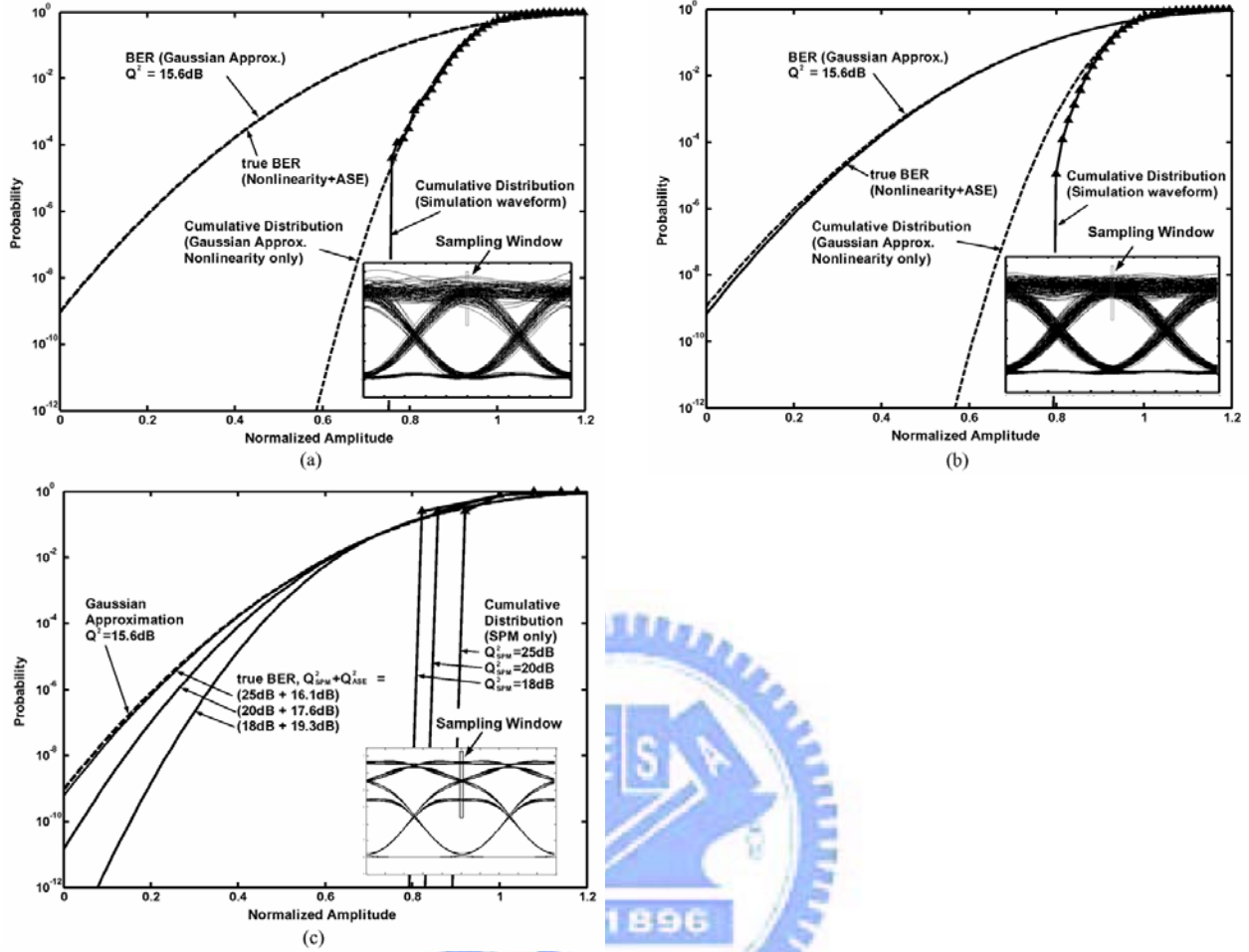
Fig. 3 Cumulative waveform amplitude distribution of simulated nonlinear interference/distortion obtained at an optimum sampling point, for the central 4 channels of a U-DWDM system. The result is a distribution of 50 independent simulations. Dashed curves are Gaussian Approximation.

(a) (FWM-dominant) 2.5Gbps/6.25GHz system after 5400km SMF transmission, corresponding to the 40km-span, DCR=93% point in Fig. 7(a). 51,200 symbols, Q^2=21.5dB.
(b) (SPM, XPM-dominant) 10Gbps/25GHz system after 4,000km NZDSF (D=6psec/nm/km), corresponding to the 40km-span, DCR=90% point in Fig. 11(a). 204,800 symbols, Q^2=21dB.
(c) (SPM-dominant) Comparison between Gaussian approximation and the true distribution. The true BER's (solid curves) are obtained by using the method given in Appendix.

Note that space level impairment is dominated by deterministic distortions due to linear dispersion. Spontaneous-spontaneous emission beat noise and nonlinearity are negligible at space level. Space-level deterministic distortion is taken into account in our calculations and simulations by replacing m_0 in (1) with the highest distorted space amplitude. Therefore, the effect of liner dispersion-induced ISI on (1) is to effectively introduce additional eye-opening penalty.

- 8 -

To verify the validity of treating optical nonlinearities as random noise in (2), under the conditions of a relatively large Q^2 and the fact that the variance of these impairments are smaller than that of ASE, Fig.3 shows the amplitude distributions of mark of simulation data at the optimum decision point of received eye diagrams.   Fig. 3(a) shows the amplitude distribution in a 40-channel 2.5Gbps/6.25GHz system transmitted over 5400km SMF with DCR=93% (corresponding to the point shown in Fig. 7(a)).   The result is a distribution of 51,200 symbols, which were obtained from the central 4 channels (256 symbols per channel) and 50 independent simulations.   The average Q^2 is 21.5dB and is dominated by FWM.   Dashed curves are Gaussian approximation with the same Q^2.   We can see that the FWM amplitude distribution matches very well with the Gaussian approximation.   This is because the dominant interference is contributed from many different independent channels via FWM.   Because of finite U-DWDM channels and simulation symbols, the cumulative distribution of the simulated waveform (excluding ASE noise) deviates away from Gaussian approximation at the tail.   However, when ASE noise is added, the true BER (solid curve, the cumulative distribution calculated based on a method detailed in Appendix A [25, 28]) and BER with Gaussian approximation (dashed curve) match each other extremely well.   Fig. 3(b) shows the amplitude distribution in a 40-channel 10Gbps/25GHz system transmitted over 4000km NZDSF with 6 ps/nm/km fiber dispersion and DCR=93% (corresponding to the maximum transmission distance in Fig. 11(a)).   The result is a distribution of 204,800 symbols, which were obtained from the central 4 channels (1,024 symbols per channel) and 50 independent simulations.   The average Q^2 is 21dB and is dominated by SPM and XPM (see Fig.11(b)).   Although a slight deviation from Gaussian distribution is observed, the distribution can be brought closer to Gaussian when ASE noise is added (see the cumulative distribution (BER) curve with ASE noise included).   Noise and nonlinearities on space level are neglected and not shown in the above figures. Fig. 3(c) shows the amplitude distribution when SPM-induced waveform distortion is the dominant impairment.   We checked an extreme case, in which the mark level is split into 3 levels due to SPM (see the eye diagram shown in the inset of Fig.3(c)).   We assume the three levels are binomially distributed with probabilities of 1/4, 1/2, and 1/4, representing the probabilities of bit sequences "00", "10" or "01", and "11", respectively.   Because SPM results in deterministic waveform distortion, they cannot be approximated as Gaussian noise.   However, when ASE noise with the same order of magnitude is added, the situation is different.   The true BER (solid curves) are obtained with a method detailed in Appendix A.   The Gaussian approximation by treating SPM as a normal variance in (2) is shown as dotted curve.   Three different values of $Q^2{}_{SPM}$, 18, 20 and 25dB are shown in the figure.   The corresponding $Q^2{}_{ASE}$ are chosen so that the combined $Q^2{}_{SPM+ASE}$ = 15.6dB.   We can see that, although a large deviation between Gaussian approximation and the true BER occurs when $Q^2{}_{SPM} < Q^2{}_{ASE}$, Gaussian approximation matches very well with the corresponding true BER when $Q^2{}_{SPM} > 25$dB.   As we will see the in Section III (Fig.11 and 12),

$Q^2_{SPM} > 25dB$ is generally satisfied in our calculations/simulations, especially in the region near the optimum DCR.

In the followings, we will concentrate on analytical tools for each individual fiber-nonlinearity-induced interference or distortion, and linear-dispersion induced ISI.   In Section III, we will add amplifier noise in the overall system performance evaluation.

2.1.1 Four Wave Mixing

In an amplified and dispersion compensated DWDM system, FWM terms generated at every amplifier stage are added according to their phase relations.   Starting from the coupled nonlinear Schrödinger's equations (NLSE) with three CW wavelengths located in f_i, f_j and f_k and applying the general system model as shown in Fig.2(a), we can get a general form of FWM in E-field at a frequency $f_{FWM} = f_i + f_j - f_k$ and a distance $L_T = \sum_{n=1}^{N} L^{(n)}$ [24, 29-31].

$$E_{FWM,ijk}(L_T) = d \cdot E_i E_j E_k^* \cdot \sum_{n=1}^{N} \left\{ \begin{array}{l} \gamma^{(n)} \exp\left[-\sum_{\ell=1}^{n} \frac{\alpha^{(\ell)}}{2} L^{(\ell)} \right] \prod_{\ell=1}^{n} \sqrt{g^{(\ell)}}^3 \cdot \exp\left[\sum_{\ell=1}^{n-1} \left(-\alpha^{(\ell)} L^{(\ell)} + i\Delta\beta^{(\ell)} L^{(\ell)} \right) \right] \\ \cdot \left[\frac{\exp\left(-\alpha^{(n)} L^{(n)} + i\Delta\beta^{(n)} L^{(n)} \right) - 1}{-\alpha^{(n)} + i\Delta\beta^{(n)}} \right] \end{array} \right\} \tag{3}$$

where $\left| E_{FWM,ijk}(L_T) \right|^2 = P_{FWM,ijk}(L_T)$ is the FWM power, $\left| E_{i,j,k} \right|^2 = P_{i,j,k}$ is the launched CW signal power at frequencies $f_{i,j,k}$; d is the degeneracy factor ($d = 1$ for $i = j$, and $d = 2$ for $i \neq j$). $\gamma_i^{(n)} = \frac{2\pi n_2^{(n)}}{\lambda A_{eff}^{(n)}}$ is the fiber nonlinearity parameter in the nth fiber section and $\Delta\beta^{(n)}$ represents the phase mismatch at nth fiber section and may be expressed in terms of signal frequency differences as

$$\Delta\beta^{(n)} = \frac{2\pi\lambda^2}{c} |f_i - f_k||f_j - f_k| \cdot \left\{ D^{(n)} + \frac{\lambda^2}{2c} \cdot \frac{dD^{(n)}}{d\lambda} \left(|f_i - f_k| + |f_j - f_k| \right) \right\} \tag{4}$$

In general, the dispersion slope term can be neglected in non-zero dispersion regions- for example, the second term due to dispersion slope in C-band is only 0.022 ps/nm/km for 25GHz spacing in NZDSF, which

is much smaller than typical $D = 2$ to 6ps/nm/km.   For periodically amplified systems without dispersion compensation, (3) can be simplified to the result given in [29] by setting $\alpha^{(n)} = \alpha$, $L^{(n)} = L$, $g^{(n)} = e^{\alpha L}$ and $\Delta\beta^{(n)} = \Delta\beta$ for all n, such that

$$P_{FWM,ijk}(N \cdot L) = \eta_{ijk}\gamma^2 d^2 L_{eff}^2 P_i P_j P_k \cdot e^{-\alpha L} \cdot \frac{\sin^2(N\Delta\beta_{ijk}\Delta L/2)}{\sin^2(\Delta\beta_{ijk}\Delta L/2)} \tag{5}$$

where $L_{eff} = \{1 - \exp(-\alpha L)\}/\alpha$ is the effective length, and η_{ijk} is the mixing efficiency given by

$$\eta_{ijk} = \frac{\alpha^2}{\alpha^2 + \Delta\beta^2}\left[1 + 4e^{-\alpha L} \cdot \frac{\sin^2(\Delta\beta L/2)}{(1 - e^{-\alpha L})^2}\right] \tag{6}$$

For systems with dispersion compensation, the accumulated phase term $\exp\left[\sum_{\ell=1}^{n-1}(i\Delta\beta^{(\ell)}L^{(\ell)})\right]$ in (3) represents the phase relation among FWM terms generated in each amplifier stage, and is proportional to fiber dispersion, channel spacing and fiber length.   For conventional DWDM systems in non-ZERO dispersion fibers, where $\Delta\beta^{(\ell)}$ is large (e.g. $\Delta\beta^{(\ell)} \approx 2\,rad/km$ for a 100GHz spaced DWDM system in NZDSF), small variation in span length $L^{(\ell)}$ can result in large phase variation in FWM terms.   Therefore, $\exp\left[\sum_{\ell=1}^{n-1}(i\Delta\beta^{(\ell)}L^{(\ell)})\right]$ was sometimes assumed to be randomly distributed over [0, 2π] and the FWM terms generated in different fiber spans are statistically power added regardless of the phase relation among stages, and the resultant FWM power is proportional to N [32].   This assumption, however, is not valid for U-DWDM systems, especially in the case of analyzing optimum DCR.   For example, consider a 6.25GHz spaced U-DWDM systems in NZDSF, $\Delta\beta^{(\ell)} \approx 0.008\,rad/km$, therefore small variations on $L^{(\ell)}$ have negligible effect on $\exp\left[\sum_{\ell=1}^{n-1}(i\Delta\beta^{(\ell)}L^{(\ell)})\right]$.   As a result, random variable assumption is not valid, and we need to use the exact form in (3), where the FWM terms generated in different fiber spans are added in E-field.

Note that the above analysis is based on three CW optical carriers without modulations.   In an M-channel NRZ modulated U-DWDM system, the total FWM at a certain channel with frequency $f_S = f_{FWM}$ is

expressed as the sum of all the FWM terms with $f_{FWM} = f_i + f_j - f_k$ in E-field [24]

$$E_{FWM} = \sum_{f_i + f_j - f_k = f_{FWM}} b_i b_j b_k \sqrt{P_{FWM,ijk}}\, e^{j\theta_{ijk}} \tag{7}$$

where $b_{i,j,k} = 1$ or 0 depending on whether the i, j, kth channel is mark or space. θ_{ijk} is the random phase of FWM terms. If the wavelengths in a U-DWDM system are equally spaced, some FWM terms will fall right below other signal bands. At the receiver, the interference on mark is originated from the beating between signal and FWM after a photodiode. The interference on space is originated from the beating between FWM terms (similar to spontaneous-spontaneous emission beat noise) and can usually be neglected in the SNR range of interest. The exact probability density functions of the FWM interference on both mark and space are detailed in [24]. It was shown in [24] that the Gaussian distribution can serve as a good approximation and the equivalent Q-factor due to FWM can be written as:

$$Q^2_{FWM}(dB) = 10\log_{10}\left(\frac{\frac{1}{2}P_S}{\overline{P}_{FWM}}\right) \tag{8}$$

where P_S is the peak received signal power per channel. $\overline{P}_{FWM} = \left\langle \left| E_{FWM} \right|^2 \right\rangle$ can be written as [24]

$$\overline{P}_{FWM} = \frac{1}{8}\sum_{f_i \neq f_j \neq f_k \neq f_{FWM}} P_{FWM,ijk} + \frac{1}{4}\sum_{f_i \neq f_j \neq f_k = f_{FWM}} P_{FWM,ijk} + \frac{1}{4}\sum_{f_i = f_j \neq f_k} P_{FWM,ijk} \tag{9}$$

where the three fractional numbers represent the probabilities of coexisting-marks among the four wavelengths (including the signal channel itself). Note that in a U-DWDM system with equal launched power per channel, $\overline{P}_{FWM} \propto P_S^3$. Therefore, according to (8), $Q^2_{FWM} \propto 1/P_S^2$.

It is a time-consuming task to calculate all the FWM terms in (9) because the number of FWM terms is proportional to the cubic of channel numbers M^3. However, a strong phase matching among the four

wavelengths (f_i, f_j, f_j and f_{FWM}) is required for the new FWM term to build up and was reflected in the FWM efficiency, (6). Note that (6) has a low-pass characteristics with a -3dB point at $\Delta f = \sqrt{\alpha \dfrac{c}{2\pi\lambda^2 D}}$, e.g. the 3dB points are about 7.3GHz and 21.2GHz for $D = 17$ and 2 ps/nm/km , respectively. This means that, first, for a U-DWDM with channel spacing close to 7.3/21.2GHz in SMF/NZDSF fibers, FWM would become very severe. Secondly, when calculating or simulating the penalty due to FWM in a U-DWDM system with a large channel count, a smaller number of closely spaced channels can possibly used to obtain the final results (with the contribution from farther away channels neglected). Using (9) we find that for a 6.25GHz channel spacing in a transmission fiber with D as low as 2 ps/nm/km, the difference of FWM power is increased by less than 1 dB when the number of channels under consideration is increased from 40 to 640 channels (fully loaded C-band). The difference is even smaller when considering SMF and larger channel spacing. Therefore, in the following analysis and numerical simulations, only up to 40 channels are used. This could save considerable computer time in Section III.

2.1.2 Cross Phase Modulation

The XPM-induced PM-to-IM interference was analyzed in frequency domain by using a modulated pump channel, k, and a CW probe channel, s, and can be written as [33-34]

$$\widetilde{P}_{XPM,sk}(L_T,\omega) = P_s(L_T)\cdot\widetilde{P}_k(0,\omega)\cdot H_{sk}^{XPM}(L_T,\omega) \tag{10}$$

where $P_s(L_T)$ is the optical power of a CW channel at a distance L_T, $\widetilde{P}_k(0,\omega)$ is the Fourier transform of the modulated pump channel, $\widetilde{P}_k(0,\omega) = \int_{-\infty}^{\infty} P_k(0,t)\cdot e^{-j\omega t}dt$, and $H_{sk}^{XPM}(L_T,\omega)$ is the normalized frequency response of the XPM induced intensity modulation from channel k to channel s and can be written as [33]

$$H_{sk}^{XPM}(L_T,\omega) = \sum_{n=1}^{N}\left\{\frac{\gamma_s^{(n)}\prod_{\ell=1}^{n-1}g_s^{(\ell)}\cdot\exp\left[\sum_{\ell=1}^{n-1}\left(-\alpha^{(\ell)}L^{(\ell)}+jd_{sk}^{(\ell)}\omega L^{(\ell)}\right)\right]}{\left(a_{sk}^{(n)}\right)^2+\left(b_s^{(n)}\right)^2}\left[\begin{array}{l}a_{sk}^{(n)}\sin\left(B_s^{(n-1)}\right)-b_s^{(n)}\cos\left(B_s^{(n-1)}\right)\\+\left[a_{sk}^{(n)}\sin\left(-B_s^{(n)}\right)-b_s^{(n)}\cos\left(B_s^{(n)}\right)\right]\exp\left(-a_{sk}^{(n)}L^{(n)}\right)\end{array}\right]\right\} \tag{11}$$

where N is the stage number in Fig. 2(a), $a_{sk}^{(n)} = \alpha^{(n)} - j\omega d_{sk}^{(n)}$, $b_s^{(n)} = \dfrac{\omega^2 D_s^{(n)} \lambda_s^2}{4\pi c}$, and

$B_s^{(n)} = \dfrac{\omega^2 \lambda_s^2}{4\pi c} \displaystyle\sum_{\ell=n+1}^{N} D_s^{(\ell)} L^{(\ell)}$. $\quad d_{sk}^{(n)} = \left(v_{gs}^{(n)}\right)^{-1} - \left(v_{gk}^{(n)}\right)^{-1} \approx D \cdot \dfrac{\lambda^2}{c} \cdot |s-k| \cdot \Delta f$ is the walk-off parameter

between channels s and k, $v_{gs}^{(n)}$ is the group velocity of channel s in the nth fiber span, and Δf is the

frequency spacing between adjacent channels. The XPM induced interference in channel s in a digitally

modulated U-DWDM system can be written as:

$$\hat{P}_{XPM,s}(L_T,t) = \hat{P}_s(L_T,t) \cdot \frac{1}{2\pi} \cdot \sum_{k \neq s} \int_{-B_e}^{B_e} \widetilde{P}_k(0,\omega) H_{sk}^{XPM}(\omega) e^{j\omega t} d\omega \tag{12}$$

where $\hat{P}_s(L_T,t)$ is the optical waveform due to residual linear dispersion at a distance L_T and is given by

[34]:

$$\hat{P}_s(L_T,t) = \frac{1}{2\pi} \int_{-\infty}^{\infty} \widetilde{P}_s(0,\omega) \cdot \cos\left(\frac{\omega^2 \lambda^2}{4\pi c}\left(\sum_{n=1}^{N} D^{(n)} L^{(n)} - PDC\right)\right) e^{j\omega t} d\omega \tag{13}$$

where $\widetilde{P}_s(0,\omega)$ is the Fourier transform of the launched intensity waveform of channel s. This general

form can be used to analyze arbitrary modulation format, DCR and PDC. We can see that the DC term of

XPM induced interference in (11) is zero and the total variance of XPM induced interference in channel s of

a U-DWDM system can be obtained by summing all the variances as

$$\sigma_{XPM,s}^2 = \sum_{k \neq s} \sigma_{XPM,sk}^2 = \frac{1}{2\pi} \cdot \left(\frac{1}{2} P_s(L_T)\right)^2 \int_{-B_e}^{B_e} \sum_{k \neq s} \left|\widetilde{P}_k(0,\omega)\right|^2 \left|H_{sk}^{XPM}(\omega)\right|^2 d\omega \quad \text{(Mark)} \tag{14}$$

$$\approx 0 \quad\quad\quad\quad\quad\quad\quad\quad\quad\quad\quad\quad\quad\quad\quad\quad\quad\quad\quad\quad\quad\quad \text{(Space)}$$

where B_e is the signal bandwidth and $\frac{1}{2}P_s(L_T)$ is the average received optical power of channel s after a transmission distance L_T.　　Accordingly, the equivalent Q^2 due to XPM only can be written as:

$$Q_{XPM}^2 = \frac{4}{\frac{1}{2\pi}\int_{-B_e}^{B_e}\sum_{k\neq s}\left|\widetilde{P}_k(0,\omega)\right|^2\left|H_{sk}^{XPM}(\omega)\right|^2 d\omega} \qquad (15)$$

We note that $H_{sk}^{XPM}(\omega)$ is a high pass transfer function, which means the variance of XPM interference in (14) is higher if the modulation signal has higher bandwidth.　　Therefore, modulation schemes with smaller bandwidths (e.g., 2.5 Gbps) are preferred to larger bandwidths (e.g., 10 Gbps) from the viewpoint of minimizing XPM interference.

In conventional DWDM systems, one can assume that exp(-αL) « 1 and the modulation bandwidth is much smaller than the channel spacing, i.e., $\omega d_{sk}^{(n)} >> \frac{\omega^2 D_s^{(n)}\lambda_s^2}{4\pi c}$, then $b_s^{(n)}$ can be neglected and (11) can be simplified to[35]

$$H_{sk}^{XPM}(L_T,\omega) = \sum_{n=1}^{N}\left\{4\gamma_s^{(n)}\prod_{\ell=1}^{n-1}g_k^{(n)}\cdot\exp\left[\sum_{\ell=1}^{n-1}\left(-\alpha^{(\ell)}L^{(\ell)}+jd_{sk}^{(\ell)}\omega L^{(\ell)}\right)\right]\frac{\sin\left(B_s^{(n-1)}\right)}{a_{sk}^{(n)}}\right\} \qquad (16)$$

However, this assumption is not valid in U-DWDM systems and the exact form (11) must be used in the following analysis.

2.1.3 Self Phase Modulation and Residual Linear Dispersion

The analytical form for XPM interference can also be used to analyze SPM distortion.　　In (11), in the limiting case when $k=s$, the normalized frequency response of SPM distortion can be written as:

$$H_s^{SPM}(L_T, \omega) = \frac{1}{2} H_{sk}^{XPM}(L_T, \omega)\Bigg|_{k=s}$$

$$= \sum_{n=1}^{N} \left\{ \frac{\gamma_s^{(n)} \prod_{\ell=1}^{n-1} g_s^{(\ell)} \cdot \exp\left[\sum_{\ell=1}^{n-1}\left(-\alpha^{(\ell)}L^{(\ell)}\right)\right]}{\left(\alpha^{(n)}\right)^2 + \left(b_s^{(n)}\right)^2} \left[\begin{array}{l} \alpha^{(n)} \sin\left(B_s^{(n-1)}\right) - b_s^{(n)} \cos\left(B_s^{(n-1)}\right) \\ + \left[\alpha^{(n)} \sin\left(-B_s^{(n)}\right) - b_s^{(n)} \cos\left(B_s^{(n)}\right)\right] \exp\left(-\alpha^{(n)}L^{(n)}\right) \end{array} \right] \right\} \quad (17)$$

The distorted pulse waveform due to ISI and SPM can be approximated as

$$\hat{P}_{SPM,s}(L_T, t) = \hat{P}_s(L_T, t) \cdot \left(1 + \Delta\hat{P}_{SPM,s}(L_t, t)\right)$$

$$= \hat{P}_s(L_T, t) \cdot \left(1 + \frac{1}{2\pi} \int_{-B_e}^{B_e} \tilde{P}_s(0, \omega) \cdot H_s^{SPM}(\omega) e^{j\omega t} d\omega\right) \quad (18)$$

In (18), $\Delta\hat{P}_{SPM,s}(L_T, t)$ is waveform distortion due to the combination of SPM and linear dispersion (similar to what was derived for XPM in (12)). In our calculations in Sec.III, SPM-limited Q^2 (Eq.(1)) will be obtained by using the mean (m_1) and variance (σ_1) at the mark level of distorted waveform (obtained from (18) at the optimum sampling point) and neglect the contribution from space level (i.e., $\sigma_0 \approx 0$). The waveform distortion at space due to linear dispersion is taken into account by replacing m_0 with the highest level at space, which causes eye–opening penalty.

2.2. Overall System Limitations

In this Section, we will calculate the overall U-DWDM system limitations by considering ISI, optical amplifier noise and all the optical nonlinearities discussed above. A generalized periodically amplified and dispersion compensated U-DWDM system shown in Fig. 2(b) is used. We assume optical amplifier gain tilts are perfectly equalized and DCFs are used for broadband dispersion and dispersion slope compensation. A tunable PDC, with continuous tuning range up to -2000ps/nm is used for individual channel performance optimization between linear dispersion and SPM/XPM. For simplicity, periodically amplified systems are assumed which have the same fiber length and DCR per span. We assume that the launched optical power into each transmission fiber span is equal, and the optical power into each DCF is 3 dB lower than the launched power to avoid additional nonlinearities generated in DCF. To focus on the fundamental system limitation due to optical fiber nonlinearities, we assumed an ideal rectangular optical filter whose bandwidth

equals to channel spacing and a receiver whose electrical bandwidth equals to 0.8 times data rate. Numerical results are obtained by solving NLSE directly by using the Split-step Fourier (SSF) method with a sampling rate of 2.56THz and 2^{18} sample points (256 and 1024 symbols per channel per simulation for 2.5 and 10 Gbps, respectively). The accuracy of the SSF method was confirmed by gradually reducing the step size. A maximum nonlinear phase change of 0.05 degree per step was used in the numerical simulation. Q^2 is calculated directly from the sample mean and standard deviation of the simulated waveform at an optimum sampling point.
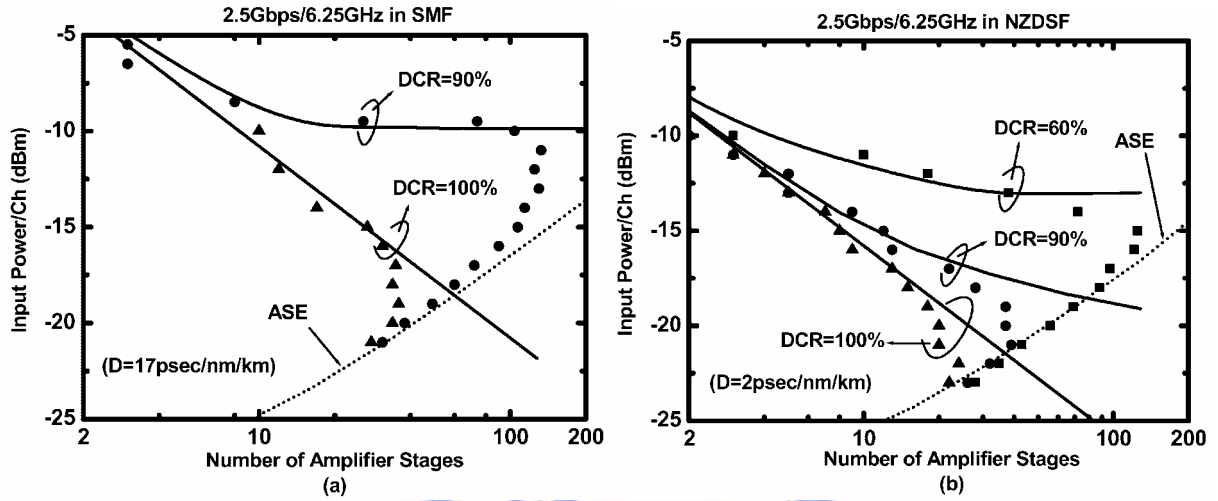
Fig. 4 FWM and ASE limited maximum fiber input power per channel of 2.5Gbps/6.25GHz systems as a function of amplifier stages for different DCR's in (a) SMF and (b) NZDSF. Assume 40km per amplifier stage. Dotted curve is ASE noise-limited minimum input power. Symbols are simulation results.

Solid and dotted curves in Figs. 3 show the calculated FWM and ASE limited fiber input powers per channel (at $Q^2(dB) \geq 15.6dB$) as a function of cascaded amplifier stages N, for 2.5Gbps/6.25GHz systems in both NZDSF and SMF. An amplifier span length of 40 km was assumed. Three different DCRs-100, 90 and 60% are shown to illustrate the effect of DCR on FWM. All symbols were obtained by choosing a specific input power/channel, and run a simulation to obtain the maximum amplifier stages which can be cascaded to reach $Q^2(dB) \geq 15.6dB$. Simulation results include all fiber nonlinearity, linear dispersion and ASE noise. Symbols near the interception points between ASE- and FWM-limited curves deviate away from their corresponding analytical FWM/ASE curves because in that region both FWM and ASE contribute to the combined Q^2 value (therefore Q^2 due to individual FWM or ASE may be a few dB greater than 15.6 dB). We can see that FWM analytical results agree very well with numerical simulation results in

2.5Gbps/6.25GHz systems in both types of fiber (Fig.4(a) for SMF and 3(b) for NZDSF).   Since numerical simulation results include all degradation factors, the results indicate that FWM is the dominant impairment in such systems.   From Fig. 4, we can see that with DCR=100%, FWM-limited launched power in NZDSF is about 5dB lower than that in SMF due to the lower local dispersion in NZDSF.   We also observe that DCR=60% offers the maximum transmission distance (= 40 km/stage × 115 stages) among the three cases in NZDSF.   The transmission distances and optimum launched powers of 2.5Gbps/6.25GHz systems in NZDSF (D=2ps/nm/km) are about 4600, 1600, 900 km and -15, -20, -22dBm for 60, 90, 100% DCR, respectively.   Similarly, the numbers for 2.5Gbps/6.25GHz systems in SMF are about 5200, 1400 km and -13, -18.5dBm for 90%, 100% DCR, respectively.

From Fig. 4, we can see that for DCR=100%, FWM-limited launched power is inversely proportional to N for both NZDSF and SMF.   This is because with DCR=100%, FWM terms generated at every amplifier stage are added in-phase according to (3).   Owing to the fact that phase matching is critical to the generation of FWM, maximum input power levels strongly depend on DCR.   For DCR other than 100%, the relation between FWM interference and stage number is not simply amplitude addition ($\propto N^2$) or power addition ($\propto N$), but depends on the dispersion map of the system.   The resultant FWM limited maximum input power at a non-100% DCR can be much higher than that with 100% DCR, especially for large number of cascaded amplifier stages.   However, even though DCR other than 100% can effectively cause the residual dispersion to suppress FWM, it can also cause pulse broadening and enhance the PM-IM conversion via SPM and XPM (which is especially critical in 10 Gbps systems).   Therefore, there exists an optimum DCR for a U-DWDM system in which FWM is dominant.   In contrast, 100% DCR is always the optimum point for a conventional DWDM system in which FWM is not the limiting factor.

From Fig. 4, we can see that as the number of cascaded amplifiers increases, the maximum FWM-limited input power decreases while the minimum ASE-limited input power increases.   Therefore, the optimum fiber input power is a balance between FWM and ASE.   With a launched power P per channel, we know from (8) that $Q_{FWM}^2 \propto 1/P^2$.   Let $Q_{FWM}^2 = K_{FWM}/P^2$ where K_{FWM} is a constant for a fixed system at a certain transmission distance and can be calculated by (8).   Similarly, we have $Q_{ASE}^2 = K_{ASE} \cdot P$ for ASE noise (assuming signal-spontaneous beat noise dominate).   In an U-DWDM system, where FWM is the dominant fiber nonlinearity, we have $\left(Q_{total}^2\right)^{-1} = \left(Q_{ASE}^2\right)^{-1} + \left(Q_{FWM}^2\right)^{-1}$ and the optimum launched power P_{opt} at a certain distance can be found by

$$\frac{d}{dP}\left[\left(\left(Q_{ASE}^2\right)^{-1} + \left(Q_{FWM}^2\right)^{-1}\right)^{-1}\right] = \frac{d}{dP}\left[\frac{1}{K_{ASE}P} + \frac{P^2}{K_{FWM}}\right] = 0 \tag{19}$$

Therefore, $P_{opt} = \sqrt[3]{1/2} \cdot P_{eq}$ or $P_{opt}(dB) \simeq P_{eq}(dB) - 1dB$, where $P_{eq} = \sqrt[3]{K_{FWM}/K_{ASE}}$ is the launched power level at which $Q_{ASE}^2 = Q_{FWM}^2$. The relation between Q_{ASE}^2 and Q_{FWM}^2 when a system is optimized is $Q_{ASE}^2(dB) \simeq Q_{FWM}^2(dB) - 3dB$. Furthermore, if we assume $Q_{total}^2 = 15.6(dB)$ at the maximum transmission distance, we find $Q_{ASE}^2(dB) \simeq 17.5dB$ and $Q_{FWM}^2(dB) \simeq 20.5dB$ at the optimum launched power. Note that this general rule holds for any $Q_{NLD}^2 \propto 1/\overline{P}_s^2$ (e.g., FWM, XPM, SPM, etc.). To show how the optimum launched power is found in a particular long-haul U-DWDM system, an example is illustrated in Fig.5. We plot the Q^2 as a function of launched optical power in a 4640 km 2.5Gbps/6.25GHz system using NZDSF fibers (D=2 ps/nm/km), with 40km per span and DCR=60%. In this case FWM is the dominant nonlinearity and the dotted line represents analytical results based on (8). As expected, the optimum launched power is a balance between ASE and FWM. The optimum launched power (P_{opt}= -15dBm) is about 1dB lower than the power (P_{eq}= -14dBm) which gives $Q_{ASE}^2 = Q_{NL}^2$. Also note that at P_{opt}= -15dBm, $Q_{ASE}^2(dB) \simeq 17.5dB$ and $Q_{NL}^2(dB) \simeq 20.5dB$, as expected.
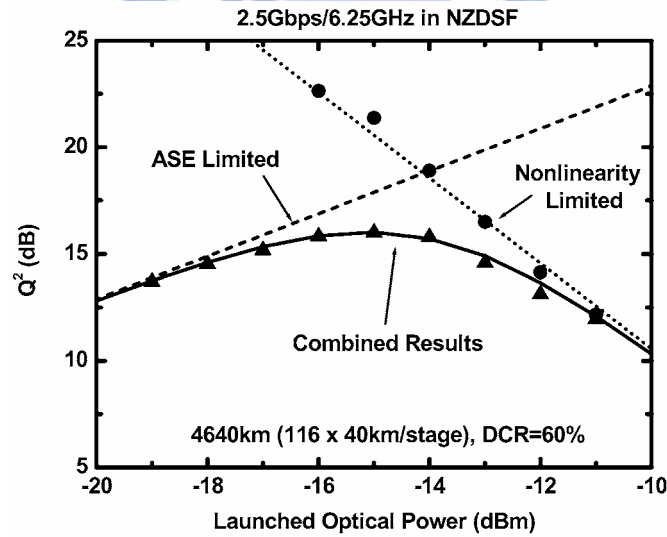
Fig. 5 Q^2 as a function of average launched optical power of a 2.5Gbps/6.25GHz system after 4640km NZDSF, which corresponds to the maximum transmission point of Fig. 6(a). Solid curve and circles are calculated and simulated received Q^2, respectively. Dotted line represents the optical nonlinearity-limited Q^2. Dashed line is ASE limited Q^2. Solid triangles are the combined results of ASE and fiber nonlinearity.

Fig.4 can be plotted in a different way, as shown in Fig.6(a), to explicitly show that the maximum transmission distance in an NRZ modulated 2.5Gbps/6.25GHz NZDSF system is obtained at optimum DCR's of about 40-60%. The maximum distance was calculated based on a received Q^2 of 15.6dB. For every DCR, the input power per channel was swept from 0 to –25dBm with a 0.5dB step size to find the maximum achievable transmission distance. Because a typical NZDSF has a dispersion value ranging from 2-6 ps/nm/km, we analyzed both the upper limit (D = 6 ps/nm/km, dotted curves) and lower limit (D = 2ps/nm/km, dashed curves), and use a solid curve to represent the worse of the two. The analytical and numerical results of maximum transmission distance for 80km-span as a function of DCR are also shown in Fig. 6(a). We can see that there exists an optimum DCR of about 40-60% and 20-40% for 40 and 80km spans, respectively, rather than ~ 100% in conventional DWDM systems. The maximum distances are about 4500 and 2300km for 40 and 80km spans, respectively. Also indicated in the same figure is the linear-dispersion limitation (dash-dotted curve) at long wavelength (D = 6ps/nm/km) and low DCR (DCR<50%) region, and is given by [36]:

$$R^2 \left(\sum_{n=1}^{N} D^{(n)} \cdot L^{(n)} - PDC \right) < 104000 \ (\text{Gb/s})^2 \cdot (ps/nm) \tag{20}$$

where R is the data rate in Gbps, $D^{(n)}$ is the fiber dispersion (ps/nm/km) of stage n, $L^{(n)}$ is the fiber span length (km) of stage n, N is the total number of stages, and PDC represents the dispersion of a post dispersion compensator (PDC = -2000ps/nm in Fig.6(a)).

Fig. 6 (a) Calculated and simulated ASE-, fiber linear dispersion- and nonlinearity-limited maximum transmission distance of 2.5Gbps/6.25GHz-spaced systems ($Q^2 \geqq 15.6$dB) as a function of in-line DCR in NZDSF. Results for both 40 and 80 km fiber spans are shown. Dashed and dotted curves were calculated based on D = 2 and 6 ps/nm/km, respectively, while solid curves represent the worse of the two. ● and ▲ are simulation results. In-line DCFs are used for dispersion compensation and the input power into DCF is 3dB lower than that into

- 20 -

transmission fiber.   A tunable PDC (up to -2,000 ps/nm) was used to optimize the individual channel performance. The dashed-dotted curve is the linear dispersion limitation at D=6 ps/nm/km.   (b)&(c) Calculated individual Q^2 for 40km fiber span.

Figs. 5(b) and 5(c) show the corresponding calculated Q^2 of individual noise and interference terms.   From Figs 5(a), (b), and (c), we can see that in a 2.5Gbps/6.25GHz system, the optimum DCR is resulted from the tradeoff between linear dispersion and FWM.   FWM is the dominant optical nonlinearity for all DCRs especially in the short wavelength region (D = 2ps/nm/km).   Note that $Q^2_{ASE} \approx 17.5dB$ and $Q^2_{NLD} \approx 20.5dB$ for all DCR>50%.   The dash-dotted curve shown in Fig 5(b) is the sum of all nonlinearity and ASE noise.   The difference between the dash-dotted and dotted curves is due to linear-dispersion-induced eye-opening penalty.   Because we use (20) as linear dispersion limitation, eye-opening penalty is kept below 1dB.   The dash-dotted curve is not shown in Fig.6(c), because in this region linear dispersion effect can be neglected.

Having discussed the maximum transmission distances of 2.5Gbps/6.25GHz systems in NZDSF, we now turn to the cases of SMF, as shown in Fig.7.   Fig.7(a) shows the linear dispersion limitation with and without PDC- we can see that the effect of PDC on the optimum DCR and maximum distance is small. This can be understood by the fact that linear dispersion limited transmission distances (dotted curves) are much longer than the maximum transmission distance at the optimum DCR.   The maximum transmission distance in SMF is about 900 and 2300km longer than that in NZDSF for 40 and 80km span length, respectively.   Fig. 7(b) shows the calculated Q^2 of individual nonlinearity, linear dispersion and ASE.   The optimum DCR is around 85-93% (Fig.7(a)), which is a trade-off among FWM, SPM/XPM and linear dispersion (Fig.7(b)).   We can see that FWM dominates in the range DCR>90%; SPM, XPM and FWM must all be considered for DCR between 80% and 90%; linear dispersion dominates for DCR<80%.
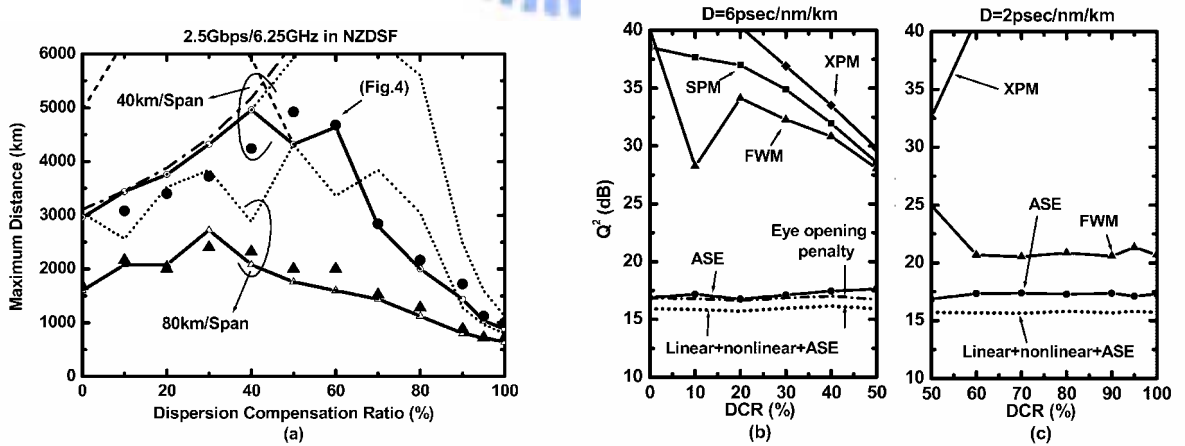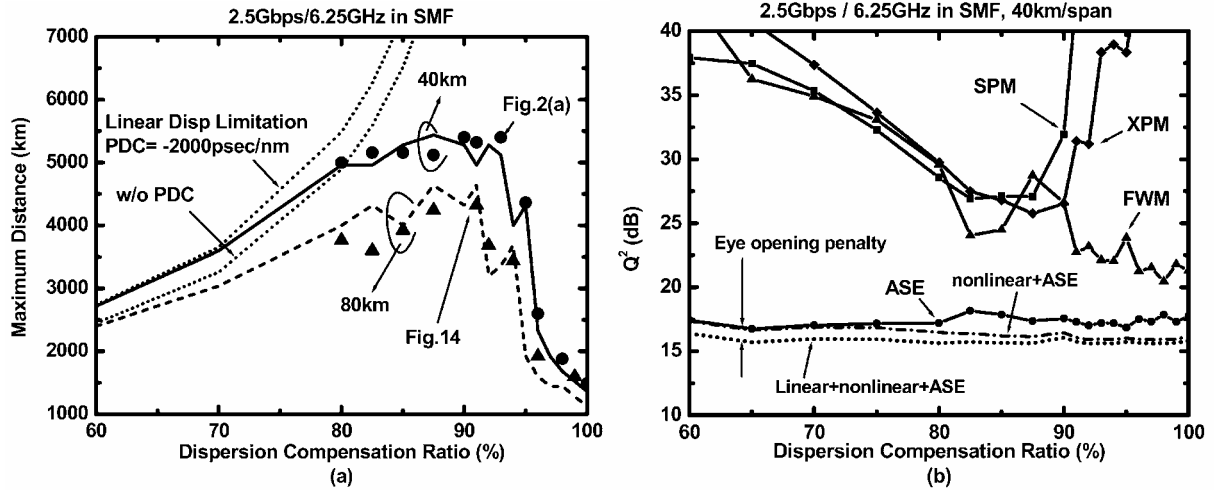
Fig. 7 (a) Calculated and simulated ASE-, fiber linear dispersion- and nonlinearity-limited maximum transmission distance of 2.5Gbps/6.25GHz-spaced systems ($Q^2 \geqq 15.6$dB) as a function of in-line DCR in SMF.   Results for both 40 and 80 km fiber spans are shown.   ● and ▲ are simulation results.   In-line DCFs are used for dispersion compensation and the input power into DCF is 3dB lower than that into transmission fiber.   A tunable PDC (up to -2,000 ps/nm) was used to optimize the individual channel performance.   (b) Calculated individual Q^2 for 40km fiber span.

Fig. 8 shows the optimum launched powers for different DCR's to achieve the maximum transmission distances given previously in Fig. 6 and 6 for NZDSF and SMF, respectively.   Note that because of the stronger FWM in NZDSF, the optimum launched power levels in NZDSF are lower than those in SMF. The optimum launched power levels in NZDSF are -15 and -12dBm at DCR = 40-60% (40km-span) and 20-40% (80km-span), respectively.   The optimum launched power levels in SMF are about -13 and -10dBm at about 85-93% DCR for 40 and 80km spans, respectively.
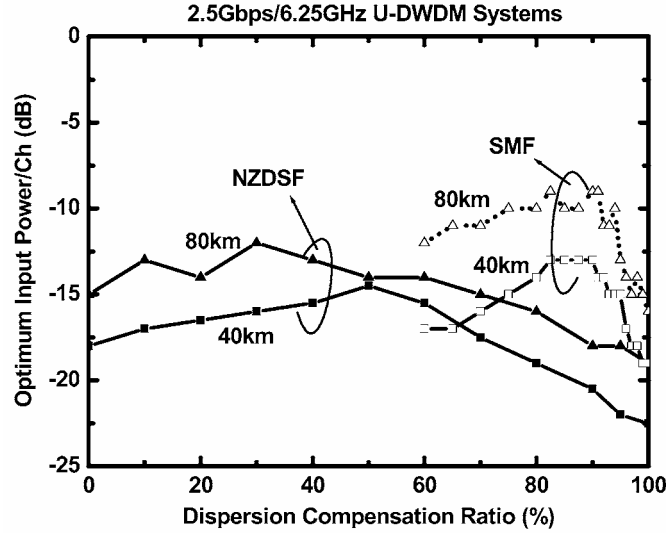
Fig. 8 Optimum launched power per channel as a function of DCR in 2.5Gbps/6.25GHz systems. The symbols correspond to the maximum transmission distances at different DCR in Fig.6(a) and Fig.7(a)

Figs. 9 (a) and (b) show fiber nonlinearities (including FWM, SPM and XPM) and ASE limited optical launched powers per channel for 10Gbps/25GHz systems as a function of cascaded amplifier stages (Fig. 2(b)) in NZDSF and SMF, respectively. Curves are calculated results based on (8), (15) and (18) for FWM, XPM and SPM, respectively; discrete symbols are numerical simulation results, which include all fiber nonlinearities, linear dispersion and ASE. Similar to Fig.4, near the interception points of nonlinearity- and ASE-limited curves, symbols deviate away from calculated results because in these regions symbols include the contributions from both nonlinearity and ASE, therefore the input power for ASE-limited case needs to be higher than that at Q^2=15.6 dB, and the input power for nonlinearity-limited case needs to be lower than that at Q^2=15.6 dB. For ideal DCR=100%, it is always FWM limited, and XPM and SPM effects can be neglected. This is clear from the good match between simulation data (▲) and calculated FWM limitations with DCR=100% in Figs. 9(a) and (b). We can see in Fig. 9(a) and (b) that XPM and SPM start to dominate over FWM after about 20 stages (800km) for DCR≠100% in both NZDSF and SMF. As opposed to a 2.5Gbps/6.25GHz system in which FWM is almost always the dominant limiting factor at optimum DCR, a 10 Gbps/25GHz system at an optimum DCR (e.g., 90% for NZDSF) must consider SPM, XPM and FWM altogether.
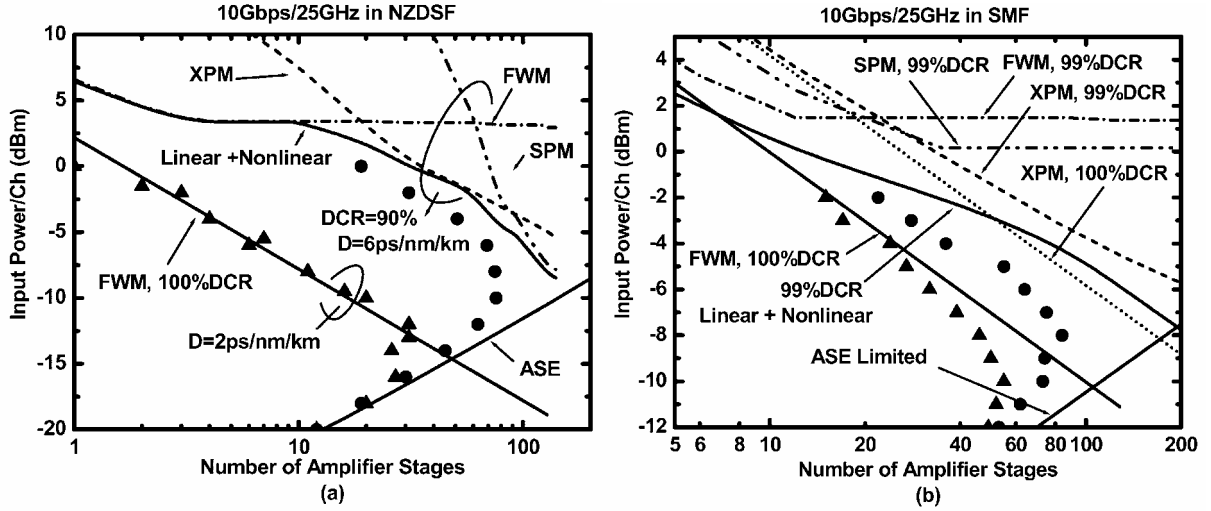
Fig. 9 Fiber input power per channel as a function of amplifier stages for different DCRs in a 10Gbps/ 25 GHz system, with 40km per amplifier stage.   Curves are calculation results, and symbols are numerical simulation results. (a) NZDSF: ▲: DCR=100%; ●: DCR= 90%;   (b) SMF: ▲: DCR=100%; ●: DCR= 99%

Results shown in Fig.9 are calculated (or simulated) with a tunable PDC before each receiver to optimize the individual 10 Gbps channel performance.   We found that there exists an optimum PDC (rather than compensating all residual dispersions) in cases where SPM or XPM cannot be neglected.   Fig. 10(a) shows an example of the eye-opening penalty due to SPM and linear dispersion as a function of PDC, in a 3600 km NZDSF (D=6ps/nm/km) with DCR=90%.   The residual dispersion in such a transmission system is 2160 ps/nm.   In the case of considering linear dispersion only (dashed curve and open symbols), the optimum PDC value is to completely compensate the residual dispersion accumulated from the non-100% DCR in every stage.   However, in the case when SPM cannot be ignored in a 10 Gbps/25GHz system due to the large PDC-dispersion-induced PM-to-IM conversion, we can find that the optimum PDC is about -1200 ps/nm instead of -2160 ps/nm.   Fig. 10(b) compares the eye diagrams obtained from calculations (using (18)) and numerical simulation.   These results show that (18) can be used as a simple and effective method to evaluate the combined waveform distortion due to linear dispersion and SPM, and in turn find the optimum PDC.   In our calculations and simulations, this optimization of PDC value has always been implemented when SPM/XPM must be considered.
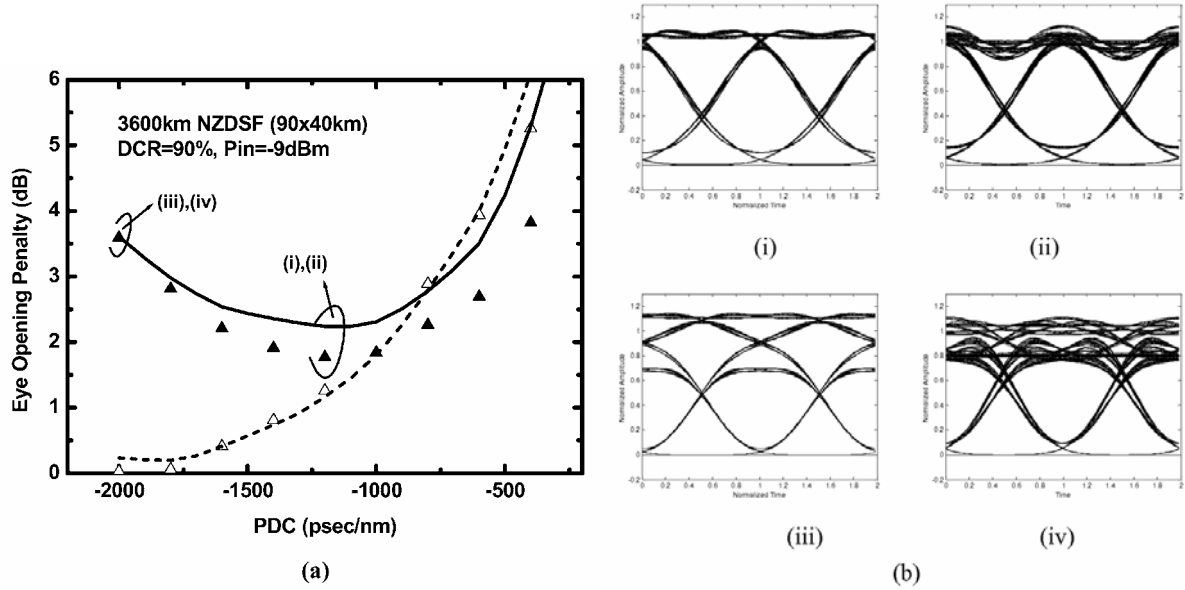
Fig. 10 Calculated and simulated Eye-opening penalty due to SPM and linear dispersion as a function of PDC. Assume a single channel 10Gb/sec system over 3600km of NZDSF fiber (D=6ps/nm/km). DCR=90%. (a) Solid and dashed curves are calculated eye-opening penalties due to SPM+linear dispersion and linear dispersion only, respectively. ▲ and △ are simulated eye-opening penalties due to SPM+ linear dispersion and linear dispersion only, respectively. (b) Eye diagrams obtained via calculations ((i) and (iii)) and simulations ((ii) and (iv)).

The maximum transmission distance of a 10Gbps/25GHz NZDSF system is shown in Fig. 11(a). Similar to Fig. 6(a), maximum distance limitation in both D= 2 and 6 ps/nm/km regions are shown in the figure. We can see that the optimum DCR is quite different from those of 2.5Gbps/6.25GHz systems in Fig. 6(a). This is because 10Gbps systems are much more sensitive to fiber dispersion, even though the larger channel spacing can reduce various fiber nonlinearity-induced impairments. The maximum transmission distance is about 3800 km and 3000 km with optimum DCR's of 90-95 and 86-91% for 40 and 80km spans, respectively. Note that the optimum DCR is under the assumption that the PDC is capable of compensating any residual dispersion lower that 2000 ps/nm.

In Fig.11(a), the linear dispersion limitations (dash-dotted curves) are calculated in the long wavelength region (D = 6 ps/nm/km). We notice that when there is no PDC applied, two negative impacts are incurred. The first is that the maximum transmission distance is reduced to about 3000 (from 3800) and 2200 (from 3000) km for 40 and 80km span, respectively. The second is that the optimum DCR for both spans is narrowed down to a sharp range of about 96%, as opposed to the original 90-95% range when –2000 ps/nm PDC was used. This sharp range of optimum DCR is not practical in real-world systems. Fig. 11(b)

shows the corresponding Q^2 for individual limiting factors in short wavelength region (D = 2ps/nm/km) for DCR$\geq$91% and long wavelength region (D = 6ps/nm/km) for DCR$\leq$90%.   We find that the dominant fiber nonlinearities are XPM and SPM in the higher dispersion region; and FWM in the lower dispersion region.
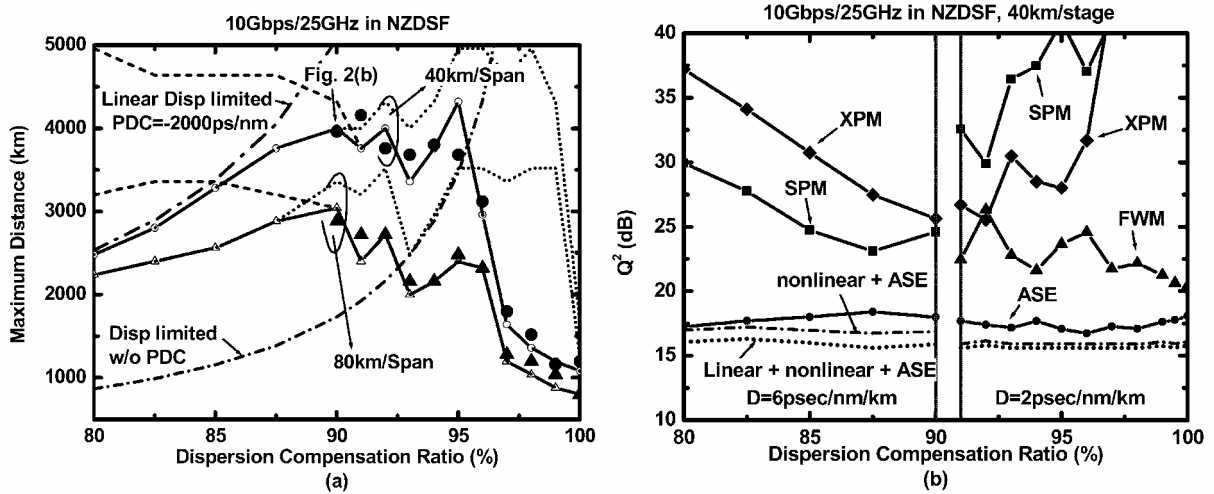
Fig. 11 (a) Calculated and simulated fiber linear-dispersion- and fiber nonlinearity-limited maximum transmission distance of a 10Gbps/25GHz system (Q^2=15.6dB) as a function of in-line DCR in NZDSF.   Solid curves are analytical results for 40 and 80km fiber spans with dashed and dotted curves for D = 2 and 6 ps/nm/km, respectively. ● and ▲ are simulation results with 40 and 80km fiber span, respectively.   In-line DCFs are used for dispersion compensation and the input power into DCF is 3dB lower than that into transmission fiber.   A tunable PDC (up to -2,000 ps/nm) was used to optimize the individual channel performance.

(b) Calculated, corresponding individual Q^2 of 40km fiber span.   The results shown are calculated with D=6 and 2 psec/nm/km for DCR$\leq$90% and DCR$\geq$91%, respectively.

Fig. 12(a) shows the transmission system performance of 10Gbps/25GHz system in SMF.   The calculated and simulated maximum distances are obtained with a -2000ps/nm tunable PDC to optimize system performance.   The optimum DCR for 10Gbps/25GHz systems in SMF is 98-99% because of the larger fiber dispersion.   Note that in this case, the optimum DCR range is already very narrow.   When no PDC is used, shown by the dotted line w/o PDC in Fig.12(a), this range will be even narrower.   Figs. 12(b) and(c) show the individual Q^2 due to various impairments for 40 and 80 km spans, respectively.   We can see that SPM and XPM are the two main limiting fiber nonlinearities in a 10Gbps/25GHz system in SMF.   For DCR<90%, the transmission distances are limited by linear dispersion.
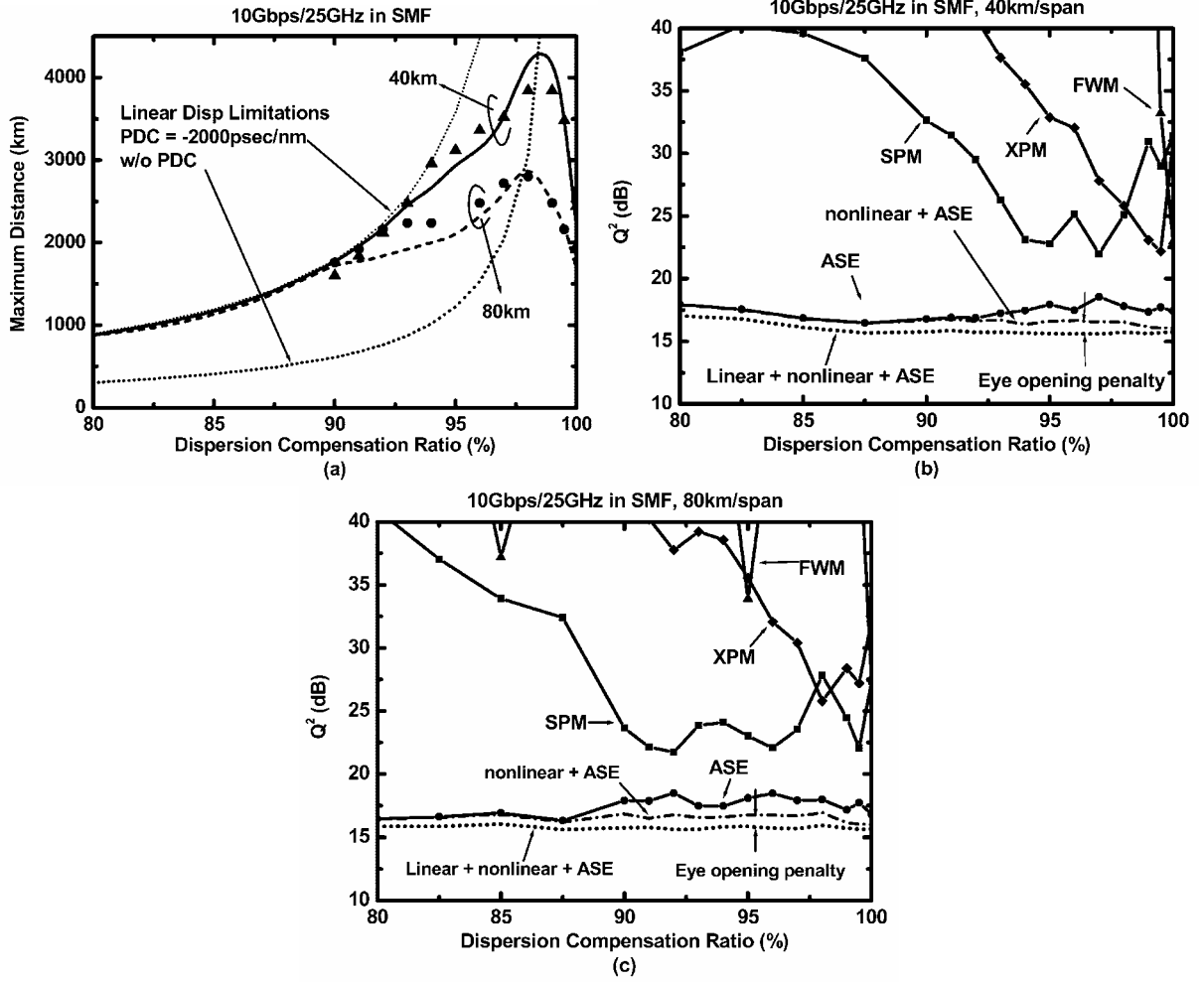
Fig. 12 (a) Calculated and simulated fiber linear dispersion- and nonlinearity-limited maximum transmission distance of 10Gbps/25GHz systems ($Q^2 \geqq 15.6$dB) as a function of in-line DCR in SMF.   Solid and dashed curves are analytical results for 40 and 80km, respectively.   ● and ▲ are simulation results with 40 and 80km fiber spans, respectively.   In-line DCFs are used for dispersion compensation and the input power into DCF is 3dB lower than that into transmission fiber.   A tunable PDC (up to -2,000 ps/nm) was used to optimum the individual channel performance.   (b)&(c) Calculated corresponding individual Q^2 of 40&80 km fiber span, respectively.

Fig. 13 shows the calculated optimum PDC (corresponding to the maximum distances in Figs. 11(a) and 11(a)) as a function of DCR.   In our calculations and simulations, we assumed that the maximum PDC is up to -2000ps/nm.   From (20), a PDC can increase the transmission distance by $\Delta L = \dfrac{PDC}{D \cdot (1 - DCR)}$ for a system limited by linear dispersion (i.e., in the region DCR < 95 and 85% for SMF and D=6ps/nm/km NZDSF, respectively).   However, when a system is limited by fiber nonlinearity instead, increasing PDC is not going to be useful (i.e., in the region DCR > 95 and 85% for SMF and D=6ps/nm/km NZDSF, respectively).   Judging from Figs. 11(a) and 12(a), which show that the optimum DCR's are about 90-95% and 98-99% for NZDSF and SMF, respectively, -2000 ps/nm PDC is quite sufficient for both types of fibers.
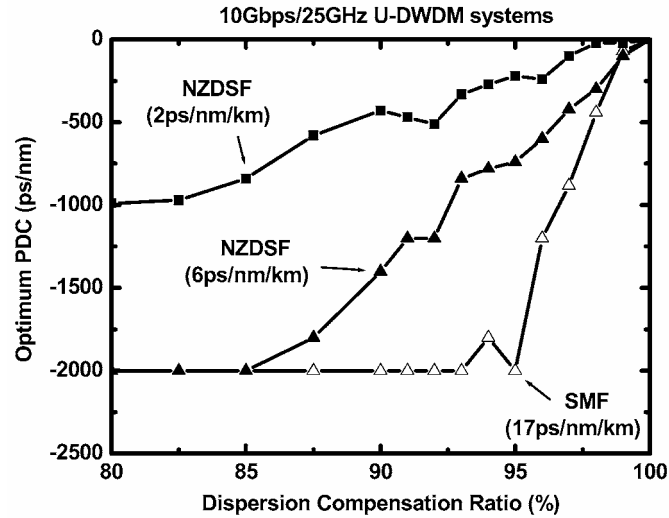
Fig. 13 Calculated optimum PDC as a function of dispersion compensation ratio at the optimum transmission distances in Fig. 11(a) and 12(a)

Fig. 14 shows the optimum launched power per channel of 10Gbps/25GHz systems in both NZDSF and SMF. The optimum launched powers in NZDSF are about -10 and -6 dBm (at DCR = 95 and 90%) for 40km and 80km spans, respectively. The optimum lunched powers in SMF are about -8 and -4dBm (at DCR=99 and 98%) for 40km and 80km spans, respectively.
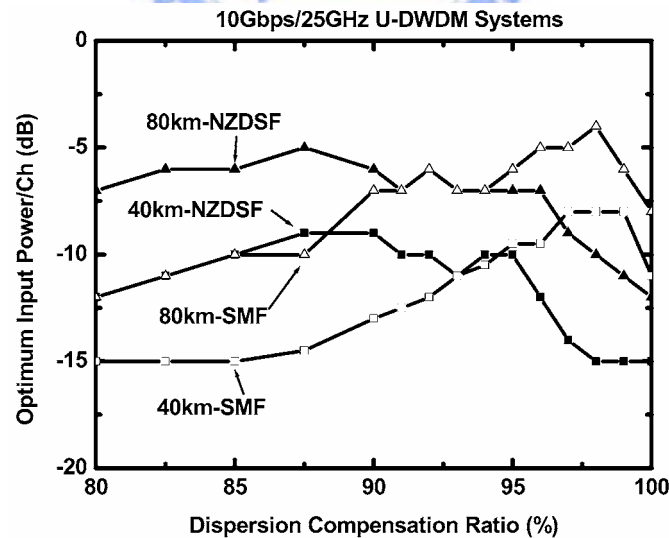
Fig. 14 Optimum launched power per channel as a function of DCR, corresponding to the maximum transmission distances at the various DCR's in Fig.10(a) and Fig.11(a)

2.3. Discussions

The results obtained in this work are based on the assumption of being able to use ideal rectangular optical filters.   However, it is well-known that filter shape and bandwidth have significant effect on ISI and adjacent channel interference, especially in U-DWDM systems [5, 37].   Furthermore, when the interplay between filters and fiber nonlinearities are considered, the problem becomes even more complicated and no analytical forms are yet available for system optimizations [27].   Therefore, more investigations need to be carried out to understand the optimum filter design for U-DWDM systems.

One may find that the calculated maximum transmission distances in Section III are shorter than some published experiment results [2-3].   The main difference is because Q^2=15.6dB was used in all calculations in this work which leaves a reasonable margin for practical system operation with FEC (e.g. a 5 dB coding gain for typical RS(255,239)); while in most previous experiments, the transmission distances were pushed to the limit with a more powerful FEC and without any operating margin.   Secondly, in our calculations, all channels were assumed to have the same polarization, while polarization interleaving was used in most published experiments.   Polarization interleaving can reduce fiber nonlinearity-induced interference between channels, therefore, the net effect of a polarization interleaved DWDM system with Δf channel spacing will be equivalent to the case of a channel spacing between Δf and $2\Delta f$.   Nevertheless, we believe the assumptions used in this paper fit practical system conditions better.

An interesting phenomenon we found is that Q^2 of U-DWDM systems are not always monolithically decreasing as a function of distance because of the resonance effect of FWM [29].   The FWM resonance can be illustrated with Fig. 15.   Fig. 15(a) shows calculated and simulated Q^2 as a function of transmission distance in a 2.5Gbps/6.25GHz system with 80km SMF span and 91% DCR (corresponding to the maximum distance point in Fig. 7(a)).   From the calculation, we know that the Q^2 is dominated by ASE and FWM.   According to (3), the resonance period of FWM in a periodically amplified DWDM system can be calculated by

$$\Delta\beta \cdot (1 - DCR) \cdot N \cdot L = 2\pi \quad (DCR \neq 100\%) \tag{21}$$

(21) means the phase of FWM interference generated in the N amplifier stages are equally distributed over 0 to 2 π, which minimizes the added phasor in (3).   Using (21), we can get a period of $N \cdot L \simeq 2089$ km as

shown in the Fig. 15. The calculated and simulated results were double checked by a commercial optical system simulation software-VPI-TransmissionMaker and the results show good match with both our analysis and simulation. We find that the simulation results do not have resonance peaks as strong as those of analytical results, especially after long transmission distance. This is because the analytical solutions are derived by CW FWM with a probability of coexisting marks; while in real system, NRZ-modulated signal has a ±2.5 GHz frequency spread around the center wavelength, which randomizes the phasor in each amplifier stage slightly (e.g., $\Delta\beta^{(\ell)} \approx 0.008\,rad\,/\,km$ in Sec.IIA can be varied slightly to $\Delta\beta^{(\ell)} \approx 0.004 \sim 0.014 rad\,/\,km$). Nevertheless, we can see the simulation results match very well with analytical results. It should be cautioned that, due to this resonance effect, there is a wide range of transmission distance that exhibits a Q^2 value close to 15.6 dB (e.g., from 3000 to 4000km in Fig.15). Therefore, using Q^2=15.6dB as a hard cutoff criterion to find the maximum transmission distance may not be quite appropriate in this case.
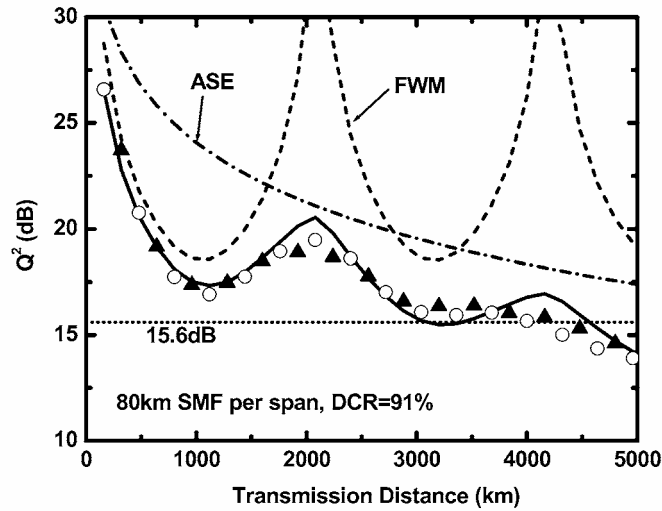
Fig. 15 Q^2 as a function of transmission distance when FWM and ASE dominate. Assume a 2.5Gbps/6.25GHz system in SMF with span=80km and DCR=91%. Curves are analytical results for Q^2_{FWM} (dashed), Q^2_{ASE} (Dash-dotted) and $Q^2_{FWM+ASE}$ (solid). ▲ and ○ are simulation results with split-step FFT method and with commercial simulation software- VPI-TransmissionMaker, respectively.

2.4. Conclusions

We have analytically and numerically investigated the transmission performance of 2.5 and 10 Gbps U-DWDM systems with a spectral efficiency of 0.4 bit/sec/Hz. Numerical simulations confirmed that the transmission system performance can be accurately predicted by using analytical equations for individual optical nonlinearity in both conventional single mode fiber (SMF) and non-zero dispersion shifted fiber (e.g.,

- 30 -

LEAF or TrueWave fiber). The optimum launched power, maximum transmission distance with dominant nonlinearities and the corresponding DCR in various systems are summarized in Tables 2 and 3, respectively. Generally speaking, the optimum launched power is higher and the maximum distance is longer in SMF than those in NZDSF. We observe that in all U-DWDM systems, there exists an optimum DCR range to reach a maximum transmission distance. Most systems have a relatively manageable DCR range, except for 10Gbps/25GHz SMF system whose optimum DCR range is so narrow which may be impractical in real-world systems. We also note that due to the dispersion-sensitive nature of 10Gbps/25GHz systems, post-dispersion-compensation is required not only to increase the transmission distance, but also to increase the optimum DCR range. Table 3 also summarizes the dominant fiber nonlinearity under different system conditions. We see that in NZDSF, FWM is always the dominant nonlinearity at the optimum DCR. In SMF, however, SPM, XPM, and FWM are all important nonlinearity impairments to consider in 2.5Gbps/6.25GHz systems; and XPM is the dominant nonlinearity in 10Gbps/25GHz systems at the optimum DCR.

	Span Length	SMF	NZDSF
2.5Gbps/6.25GHz	40km	-13dBm/ch (+15dBm/640ch) @DCR=85-93%	-15dBm/ch (+13dBm/640ch) @DCR=40-60%
	80km	-10dBm/ch (+18dBm/640ch) @DCR=85-93%	-12dBm/ch (+16dBm/640ch) @DCR=20-40%
10Gbps/25GHz	40km	-8dBm/ch (+14dBm/160ch) @DCR=98-99%	-10dBm/ch (+12dBm/160ch) @DCR= 90-95%
	80km	-4dBm/ch (+18dBm/160ch) @DCR=98%	-6dBm/ch (+16dBm/160ch) @DCR= 86-91%

Table 2   Summary of optimum launch power per channel under different system conditions

	Span Length	SMF	NZDSF
2.5Gbps/6.25GHz	40km	5400km (SPM,XPM,FWM) @DCR= 85-93%	4500km (FWM) @DCR=40-60%
	80km	4600km (SPM,XPM,FWM) @DCR=85-93%	2300km (FWM) @DCR=20-40%
10Gbps/25GHz	40km	4300km (XPM) @DCR=98-99%	3800km (FWM) @DCR= 90-95%
	80km	2800km (XPM) @DCR=98%	3000km (FWM) @DCR= 86-91%

Table 3 Summary of maximum transmission distance under different system conditions

3. CSO Distortions due to the Combined Effects of Self- and External-Phase Modulations in Long-distance 1550 nm AM-CATV Systems

3.1. Experimental setup:

The experimental setup is shown in Fig. 16.   In the experiment with only a booster erbium-doped fiber amplifier (EDFA), we used an 1551.7 nm transmitter with an integrated phase modulator and a Mach-Zehnder interferometer (MZI) modulator.   The linewidth, and output power of the transmitter were 1MHz and 8.6 dBm, respectively.   The phase modulator were modulated by three tones at 1.9, 3.8, and 5.7 GHz, with β's of 3.9, 3.9 and 1.3, respectively. The resultant SBS threshold is as high as 17 dBm.   The MZI modulator was modulated by 78 AM tones from a matrix generator with an optical modulation index (OMI) per channel of 2.8%.
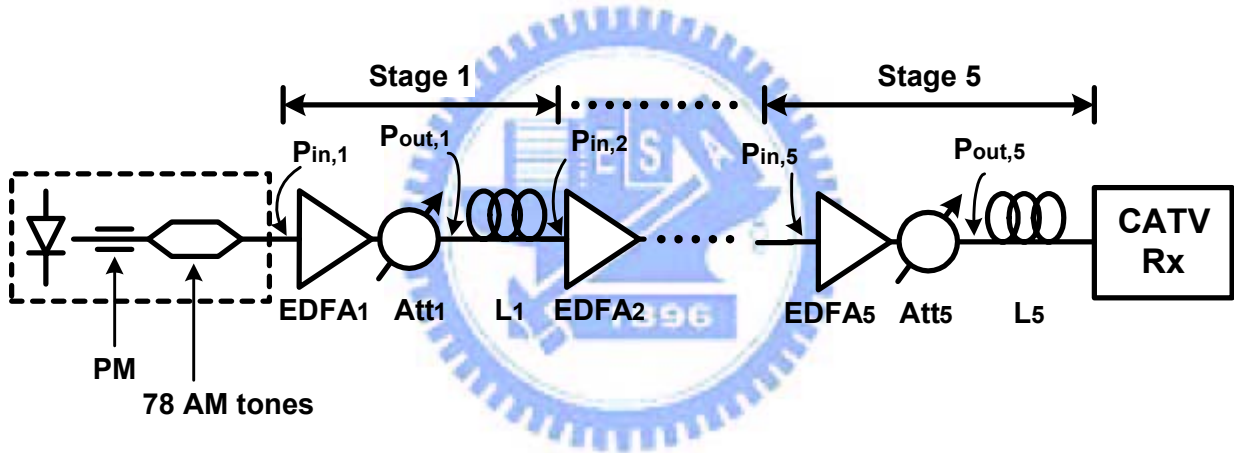
Fig. 16 Experimental Setup

In the experiment with four additional in-line EDFAs, the center wavelength, linewidth, and output power of the transmitter were 1561.1 nm, 2 MHz, and 8 dBm, respectively.   The launched optical power from each EDFA ($P_{out,i}$, i $\geq$1) was adjusted to be 12 dBm for an inter-stage optical fiber span of 60 km, and the input power ($P_{in,i}$, i $\geq$2) of each in-line EDFA was 0 dBm.   A 1.9 GHz tone with a varying rf voltage level was used to drive the phase modulator, and the combined effects of SPM and EPM at various β's were studied.

In the mean time, the CSO value at channel 2 was constantly monitored to ensure that the SBS effect could be ignored [39].   The effective core area (A_{eff}) and the attenuation (α) at 1550 nm of the transmission fiber

were measured to be 90 um^2 and 0.2dB/km, respectively.

3.2. Experimental, numerical, and analytical results

The analytical result for SPM-induced frequency-dependent CSOs is given by [8-10]

$$CSO_{SPM}(\Omega) = \left[\frac{1}{2} m \cdot \frac{\lambda^2}{2\pi c} D \cdot k \cdot n_2 \cdot \frac{P_0}{A_{eff}} \cdot \Omega^2 \cdot \overline{z^2}(L) \right]^2 \cdot N_{CSO} \tag{1}$$

where m is the OMI per channel, $k = 2\pi/\lambda$, n_2 is the nonlinear refractive index of the fiber, P_0 is the launched optical power, $\overline{z^2}(L) = (\alpha L + e^{-\alpha L} - 1)/\alpha^2$, L is the fiber length, Ω is the angular frequency at which CSO occurs; N_{cso} is the product count of second-order intermodulation products, and D is the fiber dispersion. For a long distance system with cascaded EDFAs and equal inter-stage fiber spans (EDFA gain = fiber span loss), Eq.(1) is still applicable except that the term $\overline{z^2}(L)$ should be replaced by

$\overline{z^2}(L) + (1 - e^{-\alpha L/N}) \cdot \sum_{i=1}^{N-1} \overline{z^2}((N-i) \cdot L/N)$ [9]

where N is the EDFA stages, L/N is the fiber span per stage.

Our numerical calculations, which can include both the SPM and EPM effects, are based on the split-step Fourier transform method. A sampling frequency 262.144 GHz was used to include all optical spectral components. Each CSO data is the average result of 50 times of different carrier phase combinations. The accuracy of our numerical results was confirmed by making sure that the numerical and analytical results differ by less than 1 dB when PM index $\beta = 0$.
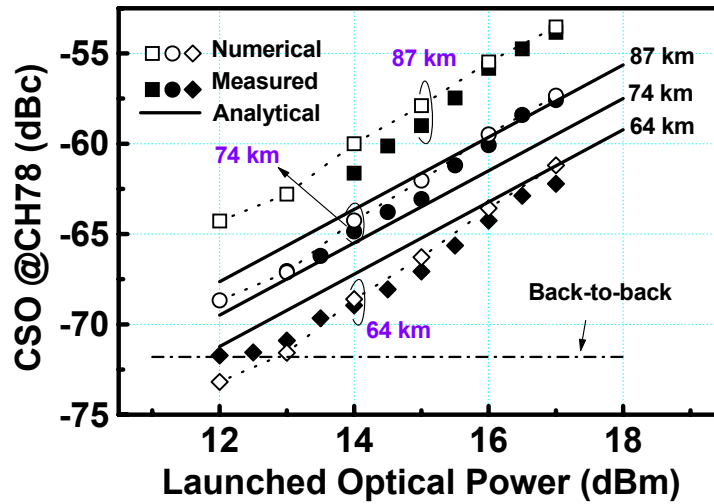
Fig. 17 CSO @ channel 78 as a function of launched optical power into a repeaterless AM-CATV system with three different transmission distances: 64, 74, and 87 km. Numerical results are for CSOs caused by both SPM and EPM effects, while analytical results are based Eq.(1). Key parameters include: OMI/ch = 2.8%, number of AM channels = 78, λ_0 = 1551.7 nm, D = 17ps/nm/km, $n_2 = 2 \times 10^{-20}$ m²/W, fiber loss = 0.2 dB/km, and A_{eff} = 90μm². β's for the three tones at 1.9, 3.8, 5.7 GHz are 3.9, 3.9, and 1.3, respectively. Soild lines, open symbols, and solid symbols represent analytical, numerical, and measured results, respectively.

For the repeaterless experiment, Fig.17 shows the worst-case CSO in channel 78 as a function of launched optical power ($P_{out,1}$, see Fig.16), for three transmission distances of 64, 74, and 87 km. We can see that the analytical results, which account for the SPM effect only, have clustered data for the three distances. While the measured and numerically calculated results spread farther than the analytical results for the three distances. It should be noted that a previous analysis of wave-envelope equation, even though with EPM included, did not find any CSO generated by the mix of EPM and intensity modulation [11]. This is probably due to the fact that the perturbation analysis in [8-10] was only up to second-order, whereas we believe that the CSOs generated by a mixing of the EPM and intensity modulation are due to higher-order nonlinearity. These CSOs due to high-order nonlinearity should not be neglected especially when (1) the transmission distance is very long, (2) the PM index β is large, and (3) the PM modulating tone frequency is very high. This conjecture was confirmed by our experimental and numerical results shown in Fig.18 and Fig.19. The measured results in Fig.18 were obtained when the fiber length and $P_{out,k}$ (k ≥1, see Fig.16) of each stage were 60 km and 12 dBm, respectively, and the total length was 300 km. We can see that the analytical results based on Eq.(1) is accurate only when the PM index β is small (e.g., β= 2.5 or 3.0) and the

transmission distance is short (e.g., < 120 km), while the numerically calculated results match well with the measured results for all β's and distances.   Note that in the case when β = 0, the analytical and numerical results match perfectly.   In Fig.19, the numerically calculated results of CSO at channel 78 versus fiber length were obtained by fixing the PM index β at 2.5, and varying the PM modulating tone frequency from 1.9 GHz to 6 GHz. We can see that in the case of the 6 GHz tone, the numerical results deviate away from the analytical results even when the distance is as short as 20 km (with a difference of about 4 dB).   In the cases of 4 and 1.9 GHz, significant differences between the numerical and analytical results start to occur at distances > 40 km and > 120 km, respectively.
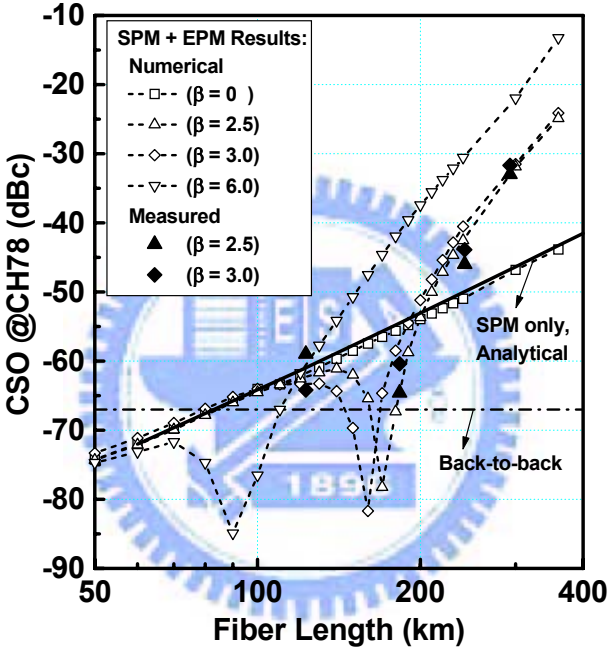
Fig. 18 Measured, numerically calculated, and analytical CSOs @ channel 78 as a function of the total fiber length in an equal-span, multi-stage-repeatered AM-CATV system. Inter-stage fiber span is 60 km.   The launched optical power from each EDFA ($P_{out,i}$, i ≥1) was 12 dBm.   (OMI/ch = 3%, λ_0 = 1561.1 nm. Single tone phase modulation at 1.9GHz. Other parameters are the same as those given in Fig. 16).
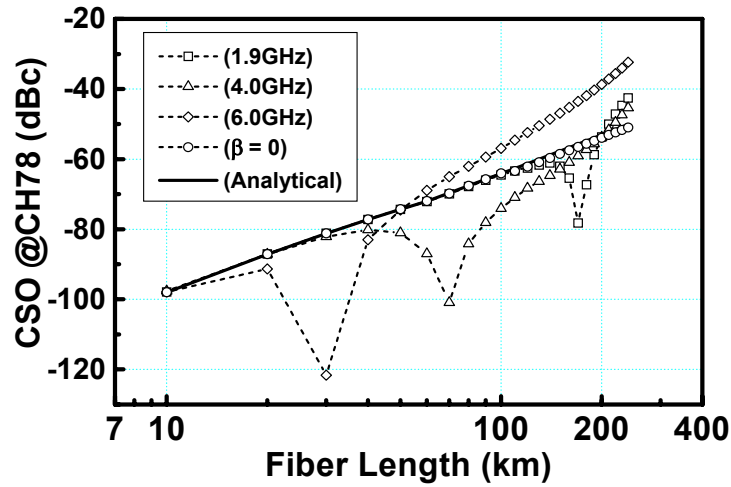
Fig. 19 Numerically calculated and analytical CSOs @ channel 78 as a function of the total fiber length in an equal-span, multi-stage repeatered AM-CATV system. (β = 2.5 for all PM modulating tone frequencies. Other parameters are the same as those given in Fig. 18)

3.3. Conclusion

By carrying out a 78-channel CATV transmission experiment with a link distance up to 300 km, and a numerical split-step transform method, we have confirmed that the CSOs can be accurately predicted by considering the combined effects of SPM and EPM. The calculated CSOs become inaccurate if one considers SPM only, especially when (1) the applied phase modulation index or tone frequency is high, and/or when (2) the transmission distance is long (e.g., around 100 km). This conclusion has important implications to the optimum design of 1550 nm transmitter for long-distance AM- and QAM-CATV transmission systems.

4. On the Validity of Using CW Tones to Test the Linearity of Multichannel M-QAM Subcarrier Multiplexed Lightwave Systems

4.1. Analysis and numerical simulation

Spectral analysis [15] has been used to calculate the NLDs induced by a general nonlinear transfer function. This analytical technique is based on the assumption that the input signal to the nonlinear device can be approximated as a Gaussian random process, and can be used to resolve all orders of NLDs by deriving from the output power spectral density (PSD).

Given a nonlinear transfer function $y = g(x)$, the signal to NLD ratio (SNLD) of the i-th channel (centered at f_i with a bandwidth $2 \cdot \Delta f$) in an N-channel SCM system can be calculated as

$$\text{SNLD}_i = \frac{b_1^2 \int_{f_i - \Delta f}^{f_i + \Delta f} |H(f)|^2 \varphi^{(1)}(f) df}{\sum_{n=2}^{\infty} \frac{b_n^2}{n!} \int_{f_i - \Delta f}^{f_i + \Delta f} |H(f)|^2 \varphi^{(n)}(f) df} \tag{1}$$

where $\varphi^{(1)}(f) = \dfrac{S_x(f)}{\int_{-\infty}^{\infty} S_x(f) df}$ is the normalized input PSD, $\varphi^{(n)}(f)$ is the n-1 times self-convolution

of $\varphi^{(1)}(f)$ ($n \geq 2$), $H(f)$ is the transfer function of the receiver baseband filter, and b_n can be evaluated from

$$b_n \equiv \frac{1}{\sqrt{2\pi}} \int_{-\infty}^{\infty} g(\sigma x) e^{-\frac{x^2}{2}} H_n(x) dx, \qquad n \geq 0 \tag{2}$$

where $H_n(x)$ is the Hermite function of n-th order and σ is the power of the input signal.   In an M-QAM demodulator, $H(f)$ is usually a Square-Root-Raised-Cosine (SRRC) filter.   However, when using multiple CW tones to characterize system linearity, $H(f)$ can generally be assumed to be a rectangular filter.

Let us assume that all M-QAM signals are 64-QAM signals with a symbol rate of 5 Msps per channel and the roll-off factor α of the SRRC filter is 0.2.   We also assume that the root-mean-squared (rms) OMI/ch

and total channel number of 64-QAM and CW tone systems are equal. Besides, both 64-QAMs and CW tones use standard NTSC frequency plan, with a bandwidth of 6MHz per channel, and a center frequency of 6X+3 MHz for 64-QAMs and a carrier frequency of 6X+1.25 MHz for CW tones.

The first case study is on laser clipping with an ideal L-I curve. In this case, it is the higher order NLDs that dominate [15]. Therefore, in calculating the total NLD power in a signal band, we have included all NLDs up to the 15-th order. Based on spectral analysis, the calculated results of using 74-channel CW tones or 64-QAM signals with rms OMI/ch=3.9% are shown in Fig.20. We can see that the resultant SNLDs in using the two different modulating signals are negligible.
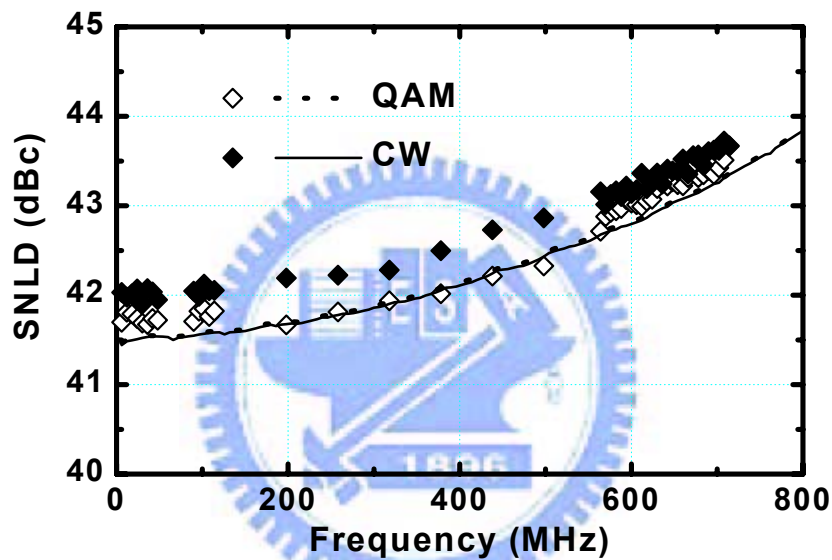
Fig. 20 Spectral analysis (solid and dotted lines) and numerical (solid and open symbols) results of LD clipping induced SNLDs. 74 channels of CW tones or 64-QAM signals were used. Number of averages were 1000 and 150 for CW and QAM, respectively. RMS OMI/ch=3.9%

Numerical simulations were used to confirm the analytical results. In Fig.20, each simulation data point is an average result of 1000 random phase combinations when using CW tones, or an average result of 150 random phase and symbol pattern combinations when using QAM signals. We can see in Fig.20 that the simulation results match very well with those of spectral analysis, and the results of using either CW tones or QAMs differ by less than 0.5 dB. Note once again that, in the case of CW tones, NLDs up to 15-th order have been included.

For the case of a directly modulated 1550nm laser passing through a span of conventional non-dispersion shifted fiber, NLDs (dominated by CSOs) generated from multi-channel CW tones or QAM signals can also

be compared.   The solid and open squares in Fig.21 are the numerically calculated SNLD caused by 74 channels of CW-tones and 64-QAM signals, respectively.   The directly-modulated 1550nm laser has a frequency chirp parameter of 3.6 GHz, and the transmission distances were 20, 40 and 80 km.   Each data point is an average result of 100 random phase combinations for CW tones, and 100 random phase and symbol pattern combinations for QAM.   As shown in the figure, the results for CW tones or QAM signals are essentially equal.

The numerically calculated results shown in Fig.21 can be checked by using a closed-form formula of CSO generated from CW tones [40] propagating in a dispersive fiber.   The solid line in Fig.21 is based on that formula and matches well with the numerical simulation results.
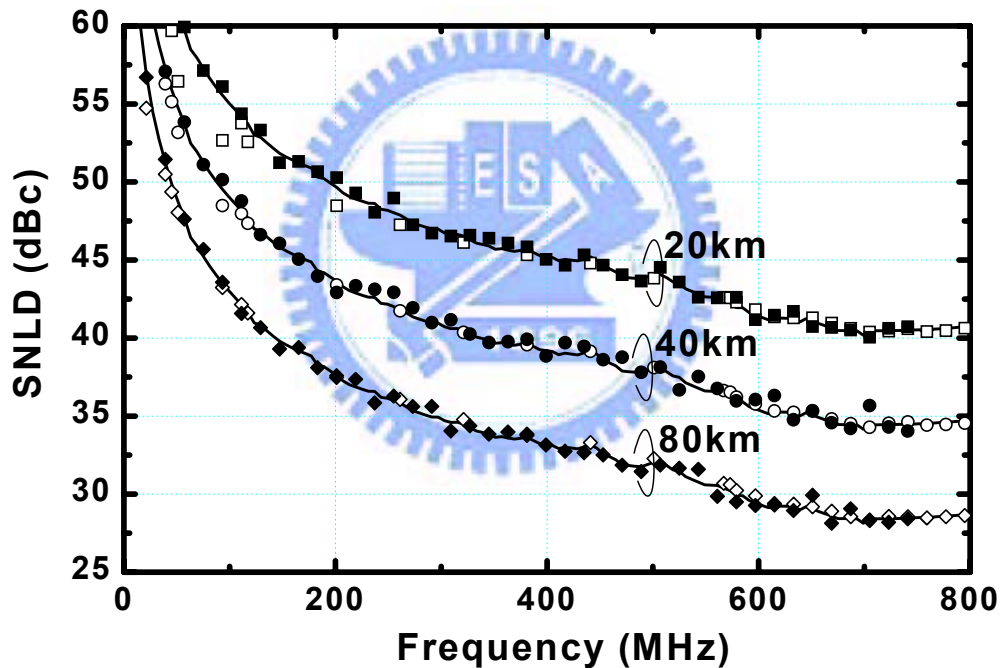
Fig. 21 Analytical (solid lines) and numerical results (open and solid symbols) of signal to second order nonlinear distortions ratio due to laser frequency chirping and fiber dispersion.   Three different fiber lengths were considered. Solid lines are calculated results based on [40]. Solid and open symbols are resulted from 74-channel CW tones and 64-QAM, respectively.

4.2. Experiment

In our experimental setup, we used 16 uncorrelated channels of 64-QAM signals (in the frequency range

258 to 354 MHz) from a vector arbitrary waveform synthesizer [15], and used 16 channels of CW tones from a matrix generator.   The measured 64-QAM signals were ensured to have a back-to-back SNR of >40 dB.   The total power of NLDs (either noise-like or discrete tones) in a 6 MHz channel was measured by using the band power measurement function of HP89440 vector signal analyzer.   When a tone-like intermodulation product occurs at the edge of a 6 MHz band, e.g., at a frequency of 6X MHz (where X is a positive integer), its power is included in the total NLD power of the signal band centered at either 6X+3 or 6X-3 MHz, but not both.

In the first part of our experiment, we compared the difference of strong laser clipping-induced NLDs due to the direct modulations of 16-channel CW tones and 16-channel 64-QAM signals, respectively.   OMI per channel ranged from 18% to 29% per channel.   The measurement results in Fig.22 show good agreement between CW tones and 64-QAMs, and agree well with the spectral analysis results.
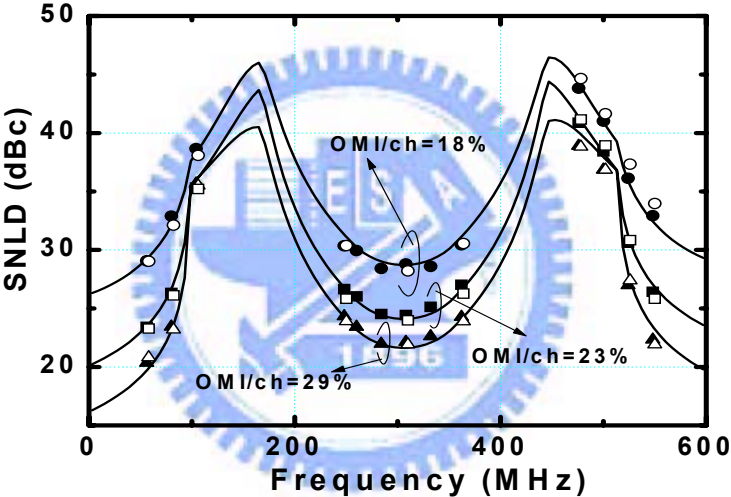
Fig. 22 Measured SNLD results for laser clipping.   Results for 16 channels of CW tones (solid symbols) or 64-QAMs (open symbols) are shown. Solid lines are calculated results based on spectral analysis.

In the second part of our experiment, we verify the difference of fiber dispersion-induced second-order nonlinear distortions when using two different types of modulating signals.   16 CW tones or 64-QAM signals with the same total rms power were used to directly modulate a 1550nm laser.   The total frequency chirp under the modulation was 3.6 GHz.   The measured results in Fig.23 show that the difference of distortions for CW tones and 64-QAMs can be less than 1dB.   Also, the calculated results based on the analysis given in [40] show good agreement with our measurement.
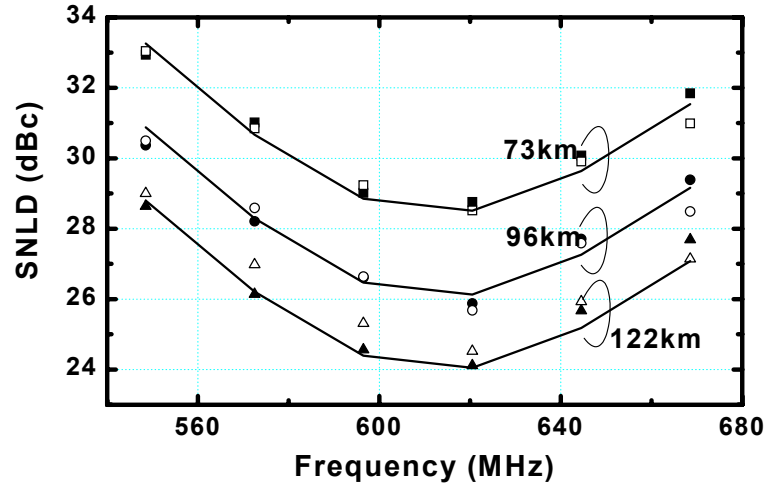
Fig. 23 Measure results of SNLD due to fiber dispersion and laser chirping for both 16-channel CW tones (solid symbols) and 64-QAM (open symbols). Solid lines are calculated results from [40]. Total laser frequency chirp is 3.6 GHz, and the fiber dispersion is 17 ps/nm/km.

4.3. Discussion

A SRRC pulse shaping filter with a roll-off factor $\alpha=0.2$ at the transmitter and a 6MHz rectangular filter at the receiver were used in all of our spectral analysis, numerical simulations and experiments. In practical M-QAM systems, however, SRRC filters are usually placed in both the transmitter and receiver ends. Therefore, the actual SNLD can be better than what we measured by about 0.33 dB.

Note that if we use CW tones as testing source, we should use a rectangular filter, rather than an SRRC filter, at the receiving end. This is because if an SRRC filter were used, it could filter out a NLD component located at a frequency equal to 6X MHz. While if a rectangular filter is used, that particular NLD component can still be counted in the total NLD. Therefore, we emphasize that all NLD components within the 6MHz band must be included when using CW tones for testing.

Another measurement issue, which needs our attention, is that the CNR of a signal generated from a practical M-QAM modulator is much lower than that from a practical CW-tone generator. The latter usually has a high CNR of > 50 dB, while the former has low CNR of about 40 dB. Therefore, when CW tones are used as the signal source to characterize system linearity, the measured SNLD must be calibrated by adding the electrical noise contributions from the M-QAM modulator to reflect what would really be measured in a multi-channel M-QAM system.

Although all experimental data in this paper were measured by the band power measurement function of HP89440, it is expected that regular spectrum analyzers can also be used. However, it should be cautioned that regular spectrum analyzers perform video average on log scale, and there is difference between *log of average* and *average of log* depending on the signal statistics [41]. For example, for Gaussian noise, there is a 2.51dB under-response by using the video average function. Since the statistics of the nonlinear distortions caused by CW tones and M-QAM's are quite different, the use of video average on a spectrum analyzer is not recommended.

4.4. Conclusions

Through spectral analysis, numerical simulations, and experiments, we found that the difference of resultant SNLDs in using multichannel CW tones and multichannel M-QAM signals is negligible, provided the following conditions can be met. The first is that both types of signal sources (having the same number of channels) have the same total rms OMI, channel bandwidth and frequency plan. The second is that all orders of nonlinear distortions in a signal bandwidth must be included in the total NLD power when CW tones are used in the measurement. Other cautions, such as do not use video average on spectrum analyzers, do not double count the CW tones-induced NLDs at the band edges, and do not neglect electrical noise contributions from M-QAM modulators, should also be carefully taken into consideration during the measurement.

5. 740 km Transmission of 78-Channel 64-QAM Signals (2.34 Gb/s) Without Dispersion Compensation by Using a Recirculating Loop
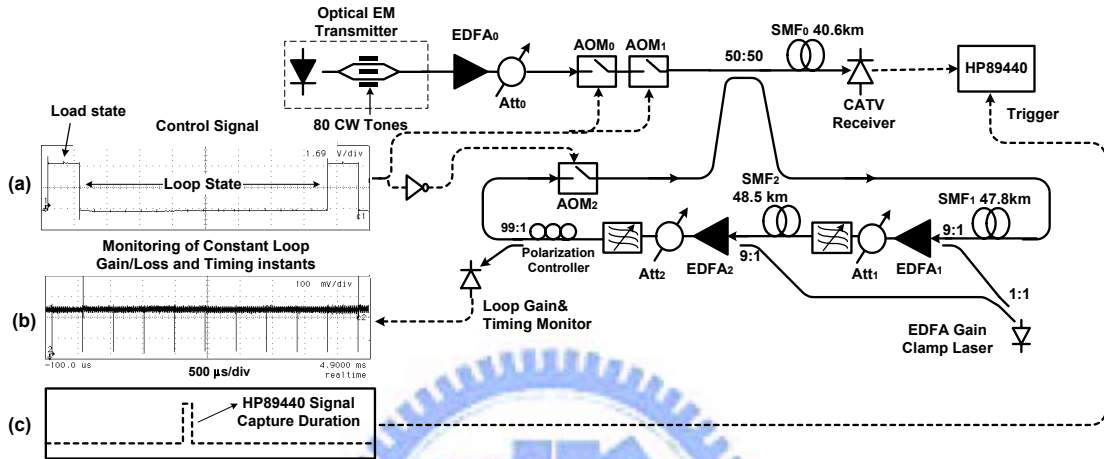
Fig. 24 Experimental setup of an SCM recirculating loop.

5.1. Experimental setup

Our recirculating loop experimental setup is shown in Fig. 24. The transmitter was composed of a 20 mW, 1561.6 nm MQW-DFB laser and a $LiNbO_3$ Mach-Zehnder (MZ) modulator. Two types of signal sources were used: 78 channels of CW tones generated from a multi-carrier generator, or 78 channels of 64-QAM signals generated from a 2.6 Gsamples/s, 8 bit/sample arbitrary waveform generator. In both cases, the 78 channels of signals ranged from 54 to 552 MHz with an rms OMI/ch given by 3.2%. For the case of CW tones, the worst case back-to-back (optical transmitter to receiver) CSO and CTB were 55 dB and 47 dB, respectively. For the case of 64-QAM signals, the back-to-back signal-to-noise ratio (SNR) per channel was about 34.5 dB. For each of the 64-QAM channels, 4096 5 Ms/s random baseband pulse-amplitude-modulation symbols with 8 levels were generated. After the constellation mapping, the symbols were split into I and Q channels. The I and Q channels were then band-limited by root-raised-cosine filters with $\alpha=0.2$. The filtered baseband waveforms were then quadrature modulated (with a random carrier phase) to the center frequency of a particular channel [22]. A total of three EDFAs were used in the experiment. $EDFA_0$ was used as a booster amplifier. $EDFA_1$ and $EDFA_2$ were used as in-line amplifiers. The noise figures of the in-line EDFAs were about 5 dB. Three spans of conventional

single mode fiber (SMF) with lengths of 40.6 km, 47.8 km and 48.5 km were used in the setup.   The fiber loss and effective core area were measured to be 0.2 dB/km and 90 μm^2, respectively.   The total fiber length per loop was 96.3 km.   To avoid fiber-dispersion-induced carrier compression effect [42], no external phase modulation was used.   Therefore the output power levels of each EDFA were maintained at   +6 dBm. The input power levels to each in-line EDFA were adjusted to be –4 dBm.   The loop gain and loss were carefully balanced, and this power balance was constantly monitored by coupling 1% optical power from the loop to a photodiode, as shown in Fig.24(b). Three acousto-optic modulators (AOMs) with 50 dB extinction ratio were used as the controlling switches to circulate the modulated light in the loop.   As shown in Fig.24(a), each cycle of the control signal was composed of a "load" state, followed by M "loop" states, where M depends on the number of re-circulation.   The duration of the load state was adjusted to be ~474 μsec, which is the time that the modulated light needed to travel through the 96.3 km loop (see Fig.24(a)). When AOM_0 and AOM_1 were ON (AOM_2 was OFF), modulated light from the optical transmitter was fed into the loop.   Following the load state were M loop states which were used to turn AOM_0 and AOM_1 off to block the signal from transmitting into the loop, and to turn AOM_2 on so as to enable signal re-circulating M times in the loop.   A gain-clamped laser was used to suppress the gain transients occurring in the in-line EDFAs.

Received signal was analyzed on a vector signal analyzer (HP89440) whose triggering time for FFT spectrum display can be controlled.   The signal capture duration of the signal analyzer was set to be 66.7 μs, as shown in Fig.25(c).   The triggering for the onset of capture time must be carefully controlled so that those transient instants shown in Fig.25(b) would not be included.   The resolution bandwidth corresponding to the 66.7 μs signal capture time was 57.3 kHz.   C/(NLD+N) per channel (6 MHz) was measured by using the band power measurement function of the vector signal analyzer.
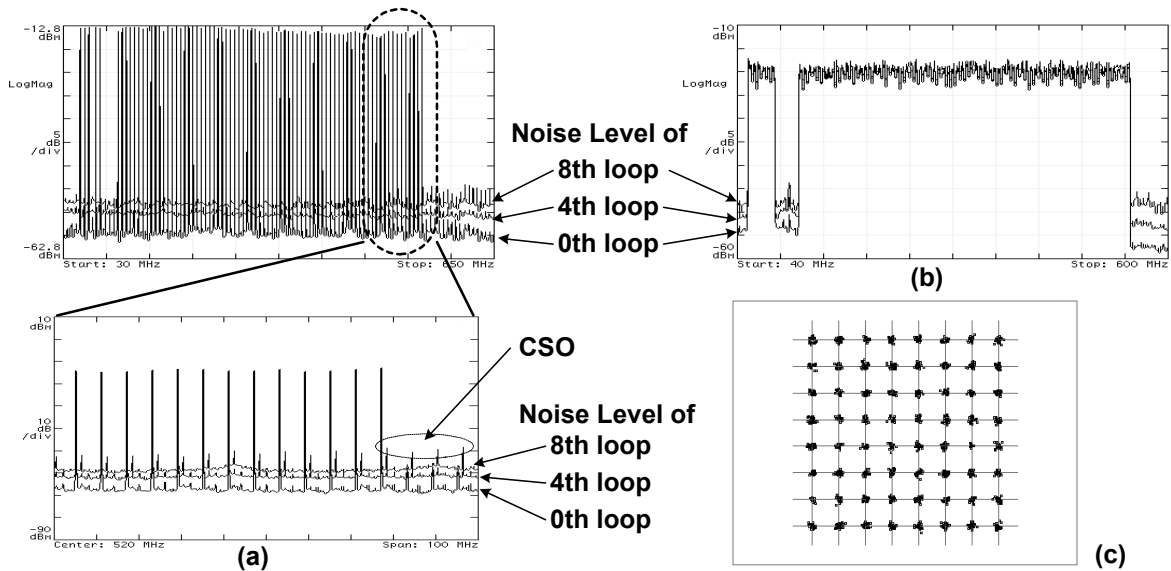
Fig. 25 Captured 78-channel CW tones (a) and 64-QAM signals (b) after 0, 4, 8 times of recirculating loops. (c) is the measured 64-QAM signal constellation diagram of channel 78 after 7 times of the recirculating loop (714 km).

5.2. Results and discussion

The measured signal spectra of the received 78-channel CW tones and 78 channels of 64-QAM signals after three looping transmission distances (40, 425, and 810 km) are shown in Fig.25(a) and (b), respectively. We can clearly see the growth of the self-phase modulation (SPM)-induced composite second-order (CSO) distortions, and the growth of total noise levels, as the transmission distance was increased. Fig.25(c) shows the measured 64-QAM signal constellation diagram of channel 78 after transmission through 7 times of recirculating loop (714 km).

In the case of transmitting 78 channels of CW tones, the measured and calculated results of CSO and CNR as functions of transmission distance are shown in Fig. 26(a). For all transmission distances, the worst-case CSO occurred at channel 78, and the measured results are shown in open circles. The corresponding calculated CSOs (solid line) were obtained by adding the back-to-back CSOs with those from the SPM analysis [43]. The deviation between calculated and measured CSOs is within 2 dB. Also shown in the figure are the measured CNRs for channels 3, 39 and 78, and the calculated CNRs for channel 78. The noise terms in these calculated CNRs include EDFA signal-spontaneous beat noise and the fiber dispersion-induced phase-to-intensity conversion noise [44]. The deviation between calculated and measured noise was mainly due to the insufficient extinction ratios of AOMs in the loop.

Fig.26 (b) is used to compare the measured C/(NLD+N) obtained from 78 CW-tones with the measured

SNRs from 78 64-QAM signals (for channels 3 and 78, respectively). Note that, for the case of CW tones, the measured (NLD+N) have included all order of nonlinear distortion and noise in a 6MHz band; while for the case of 64-QAM signals, the measured SNR was estimated by digital demodulation function of the vector signal analyzer. In addition, the artificial background noise from the AWS has been calibrated out. We can clearly see that the differences between C/(NLD+N) for tones and SNR for 64-QAM signals were within 1 dB, as has also been rigorously confirmed in [45]. According to the measured results shown in Fig.26(b), we can see that for a C/(NLD+N)$\geq$ 30 dB (required for a 64-QAM without forward-error-correction to achieve a BER of 10^{-9}), the transmission distance can be as long as ~740 km. Also shown in the figure is a solid line representing the calculated C/(NLD+N) at channel 78 (the worst-case channel) as a function of transmission distance, which was based on the calculated CSO and CNR results given in Fig.26(a).
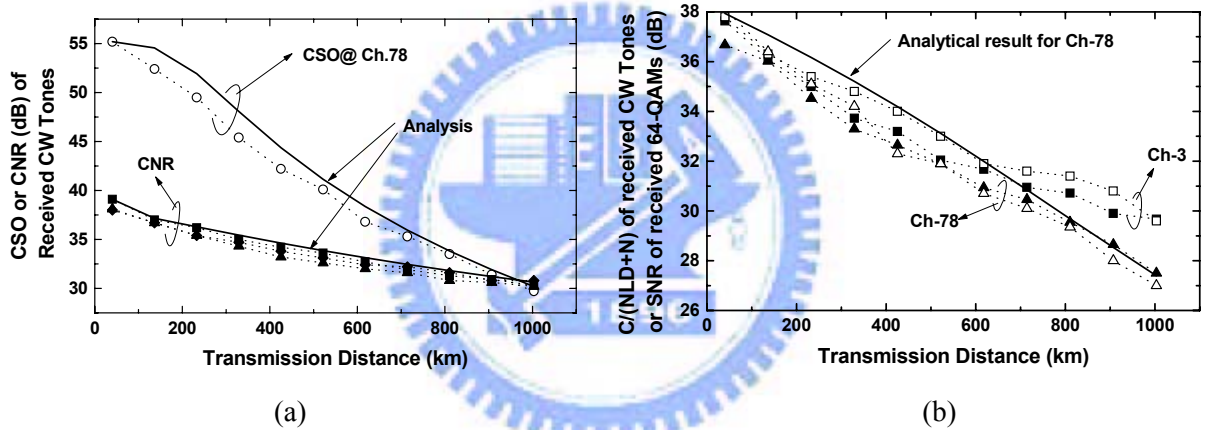
Fig. 26 (a) Measured CNR of Ch.3 (■), Ch.39(◆) and Ch.78(▲) in a 6MHz bandwidth, and the worst case CSO @Ch.78(○), for the case of transmitting 78 CW tones. (b) Measured C/(NLD+N) of Ch.3 (□) and Ch.78(△) when transmitting 78 CW tones, and the measured SNR of Ch.3 (■) and Ch.78(▲) when transmitting 78 64-QAM signals. Solid lines in (a) and (b) are the calculated results. Launched optical power was +6 dBm.

5.3. Conclusion

By carrying out a recirculating loop experiment, we have demonstrated that 1550 nm CATV external modulation systems can be used to deliver 78 channels of 64-QAM signals (equivalent to a capacity of 2.34 Gb/s) over a transmission distance > 740 km of conventional SMF without dispersion compensation. In addition, our analysis shows that, in such long distance systems, the dominant system degradation factors

include the SPM-induced second-order nonlinear distortions, the signal-spontaneous beat noise due to cascaded EDFAs, and the intensity noise converted from laser phase noise owing to the presence of significant optical fiber-dispersion.

6. Conclusions

We have analytically and numerically investigated the transmission performance of 2.5 and 10 Gbps U-DWDM systems with a spectral efficiency of 0.4 bit/sec/Hz. Numerical simulations confirmed that the transmission system performance can be accurately predicted by using analytical equations for individual optical nonlinearity in both conventional single mode fiber (SMF) and non-zero dispersion shifted fiber (e.g., LEAF or TrueWave fiber). The optimum launched power, maximum transmission distance with dominant nonlinearities and the corresponding DCR in various systems are investigated.

By carrying out a 78-channel CATV transmission experiment with a link distance up to 300 km, and a numerical split-step transform method, we have confirmed that the CSOs can be accurately predicted by considering the combined effects of SPM and EPM. This conclusion has important implications to the optimum design of 1550 nm transmitter for long-distance AM- and QAM-CATV transmission systems.

Through spectral analysis, numerical simulations, and experiments, we found that the difference of resultant SNLDs in using multichannel CW tones and multichannel M-QAM signals is negligible. By carrying out a recirculating loop experiment, we have demonstrated that 1550 nm CATV external modulation systems can be used to deliver 78 channels of 64-QAM signals (equivalent to a capacity of 2.34 Gb/s) over a transmission distance > 740 km of conventional SMF without dispersion compensation. In addition, our analysis shows that, in such long distance systems, the dominant system degradation factors include the SPM-induced second-order nonlinear distortions, the signal-spontaneous beat noise due to cascaded EDFAs, and the intensity noise converted from laser phase noise owing to the presence of significant optical fiber-dispersion.

Appendix A

In the presence of waveform distortions due to fiber nonlinearities and/or linear dispersion, marks and spaces are split into several rails. Gaussian noise is superimposed on these rails. We assume marks and spaces are split into N_1 and N_0 rails, respectively. The levels are defined as $m_{j,0}$, $m_{j,1}$, ..., $m_{j,Nj-1}$ with probability of occurrence of $m_{j,k}$ set to be $p_{j,k}$ (where k stands for the kth rail). $j = 1$ (mark) or 0 (space). In the presence of waveform distortions, BER can be obtained from [25, 28]

$$P_e(D) = \sum_{k=0}^{N_0-1} P_{0,k}(D) + \sum_{k=0}^{N_1-1} P_{1,k}(D) \tag{A.1}$$

where

$$P_{0,k}(D) = \frac{p_{0,k}}{4} erfc\left(\frac{D - m_{0,k}}{\sqrt{2}\sigma_{0,k}} \right) \tag{A.2}$$

and

$$P_{1,k}(D) = \frac{p_{1,k}}{4} erfc\left(\frac{m_{1,k} - D}{\sqrt{2}\sigma_{1,k}} \right) \tag{A.3}$$

REFERENCES

[1] H. Suzuki, M. Fujiwara, N. Takachio, K. Iwatsuki, T. Kitoh, and T. Shibata, "12.5-GHz spaced 1.28Tb/s (512-channel x 2.5 Gbps) super-dense WDM transmission over 320-km SMF using multiwavelength generation technique," *IEEE Photon. Technol. Lett.*, vol. 14, pp. 405-408, 2002.

[2] G. Vareille, F. Pitel, and J.F. Marcerou, "3 Tbit/s (300×11.6Gbit/s) transmission over 7380 km using C+L band with 25GHz channel spacing and NRZ format," *OFC 2001* , PD22 -P1-3 vol.4, 2001.

[3] C. R. Davidson, C. J. Chen, M. Nissov, A. Pilipetskii, N. Ramanujam, H. D. Kidorf, B. Pedersen, M. A. Mills, C. Lin, M. I. Hayee, J. X. Cai, A. B. Puc, P. C. Corbett, R. Menges, H. Li, A. Elyamani, C. Rivers, and N. S. Bergano, "1800 Gbps transmission of one hundred and eighty 10 Gbps WDM channels over 7,000 km using the full EDFA C-band," OFC'2000, PD25, 2000.

[4] L. Leng, S. Stulz, B. Zhu, L.E. Nelson, b. Edvold, L. Gruner-Nielsen, S. Radic, J. Centanni, and A. Gnauck, "1.6Tb/s (160 x 10.7 Gbps) transmission over 4000 km of nonZERO dispersion fiber at 25-GHz channel spacing," *IEEE Photon. Technol. Lett.*, vol. 15, pp. 1153-1155, August 2003.

[5] S. B. Jun, K. J. Park, and Y. C. Chung, "Transmission of 2.5-Gbps WDM channels spaced at 5GHz over 480 km of single-mode fiber," *IEEE Photon. Technol. Lett.*, vol. 15, pp. 1309-1311, September, 2003

[6] 21 C.Y. Kuo, D. Piehler, C. Gall, J. Kleefeld, A. Nilsson and L. Middleton, "High-performance optically amplified 1550-nm lightwave AM-VSB CATV transport system," OFC'96 Technical Digest, pp.196-197.

[7] H. Dai, S. Ovadia and C. Lin, "Hybrid AM-VSB/M-QAM multichannel video transmission over 120 km of standard single-mode fiber with cascaded erbium-doped fiber amplifiers," IEEE Photonics Technology Letters, Vol.8, pp.1713-1715, Dec. 1996

[8] M.R. Phillips, T.E. Darcie, D. Marcuse, G.E. Bodeep and N. J. Frigo, "Nonlinear distortion generated by dispersive transmission of chirped intensity-modulated signals," IEEE. Photonics Technology Letters, Vol.3, No.5, May 1991.

[9] C. Desem,. "Composite second order distortion due to self-phase modulation in externally modulated optical AM-SCM systems operating at 1550 nm, "Electron. Lett. vol 30, no 24, pp. 2055-6, Nov. 1994.

[10] Dogan A. Atlas, "Fiber induced distortion and phase noise to intensity noise conversion in externally modulated CATV systems," 1996 NCTA Technical Papers, pp.289-293.

[11] M.R. Phillips, D.W. Anthon and K.L. Sweeney, "Chromatic dispersion effect in CATV analog lightwave systems using externally modulated transmitters," OFC'96 post deadline paper PD17.

[12] F. W. Willems, W. Muys and J. C. van der Plaats, "Experimental verification of self-phase-modulation-induced nonlinear distortion in externally modulated AM-VSB lightwave

systems," OFC'96 Technical Digest, pp.281-282.

[13] 28 F. W. Willems, J. C. van der Plaats and W. Muys, "Harmonic distortion caused by stimulated Brillouin scattering suppression in externally modulated lightwave AM-CATV systems," Electronics letters, Vol.30, No.4, pp.343-345, Feb. 1994.

[14] 30 W. I. Way, Broadband Hybrid Fiber Coax Access System Technologies, Academic Press, New York, 1998.

[15] P. Y. Chiang and W. I. Way, "Ultimate capacity of a laser diode in transporting multichannel *M*-QAM signals," *J. Lightwave Technol.*, vol.15 pp.1914-1924, Oct. 1997.

[16] S. L. Woodward and G. E. Bodeep, "Uncooled Fabry-Perot lasers for QPSK transmission," *IEEE Photon. Technol. Lett.*, vol.7, pp.558-560, May. 1995.

[17] K. Maeda, M. Fuse, K. Fujito, "Ultrahigh channel capacity optical CATV systems," OFC'96 Technical Digest, pp. 197-198.

[18] 34 C. Tai, S. L. Tzeng, H. C. Chang, and W. I. Way, "Reduction of nonlinear distortion in MQW semiconductor optical amplifier using light injection and its application in multichannel M-QAM signal transmission systems," *IEEE Photon. Technol. Lett.*, vol.10, pp.609-611, Apr. 1998.

[19] 37 W. I. Way, Broadband Hybrid Fiber Coax Access System Technologies, Academic Press, New York, 1998.

[20] K. Maeda, M Fuse and K. Fujito, "Ultrahigh channel capacity optical CATV systems," OFC'96 Technical Digest, pp.197-8.

[21] S. Tsuji and Y. Hamasaki, "250 km transmission of frequency multiplexed 64-QAM signals for digital CATV backbone application," Technical Papers, NCTA, pp.21-29, May 1998.

[22] P. Y. Chiang and W. I. Way, "Ultimate capacity of a laser diode in transporting multichannel M-QAM signals," J. Lightwave Technology, vol.15 pp.1914-1924, Oct. 1997.

[23] 41 G. Wilson, "Capacity of QAM SCM systems utilizing optically linearized Mach-Zehnder modulator as transmitter," Electron. Lett., vol.34, pp.2372-2374, December 1998.

[24] K. Inoue, K. Nakanishi, K. Oda and H. Toba, "Interference and power penalty due to fiber Four-Wave Mixing in multichannel transmissions," *J. Lightwave Technology*, vol. 12, pp. 1423-1439, 1994.

[25] Seiji Norimatsu, Masanori Maruoka, "Accurate Q-factor estimation of optically amplified systems in the presence of waveform distortions," *J. Lightwave Technology*, vol. 20, pp. 19-27, 2002.

[26] Takashi Mizuochi, Kazuyuki Ishida, Tatsuya Kobayashi, Jun;ichi Abe, Kaoru Kinjo, Kuniaki Motoshima and Kumio Kasahara, "A comparative study of DPSK and OOK WDM transmission over transoceanic distances and their performance degradations due to nonlinear phase noise," *J. Lightwave Technology* , vol. 21, pp. 1933-43, 2003.

[27] Hadrien Louchet, Anes Hodzic, and Klaus Petermann, "Analytical model for the performance evaluation of DWDM transmission systems, "*IEEE, Photon. Technol. Lett.*, vol. 15, pp. 1219-21, 2003

[28] C. J. Anderson and J.A. Lyle, "Technique for evaluating system performance using Q in numerical simulations exhibiting intersymbol interference, " Electron. Lett., vol. 30, pp 71-72, Jan. 1994.

[29] D. Schadt, "Effect of amplifier spacing on Four-Wave Mixing in multichannel coherent communications," *Electron. Lett.*, vol. 27, pp. 1805-1807, 1991

[30] K. O. Hill, D. C. Johnson, B. S. Kawasaki and R. I. MacDonald, "CW three-wave mixing in single-mode optical fibers," *J. Appl. Phys.*, vol. 49, pp. 5090-5106, 1978.

[31] N. Shibata, R. P. Braun and R. G. Waarts, " Phase-mismatch dependence of efficiency of wave generation through Four-Wave Mixing in a single-mode optical fiber," *IEEE J. Quantum Electron.*, vol. QE-23, pp.1205-1210, 1987.

[32] *M. Eiselt, "*Limits on WDM systems due to four-wave mixing: a statistical approach," *J. Lightwave Technology* , vol. 17 pp. 2261-2267, 1999.

[33] Cartaxo, "Cross-phase modulation in intensity modulation-direct detection WDM systems with multiple optical amplifiers and dispersion compensators," *J. Lightwave Technology*, vol. 17, pp. 178-190, 1999.

[34] Eva Peral, William K. Marshall and Amnon Yariv, "Precise measurement of semiconductor laser chirp using effect of propagation in dispersion fiber and application to simulation of transmission through fiber grating," *J. Lightwave Technology* , vol. 16, pp.1874-1880, 1998.

[35] R. Hui; K.R Demarest, and C. T. Allen, "Cross-phase modulation in multispan WDM optical fiber systems," J. Lightwave Technology, vol. 17, pp. 1018 –1026, 1999

[36] R. Chraplyvy and R. W. Tkach, "Treabit/second transmission experiments, " IEEE J. Quantum Electronics, vol. 34, pp. 2103-2108, September, 1998

[37] Lyubomirsky, T. Qui, J. Roman, M. Nayfeh, M. Y. Frankel, and M. G. Taylor, "Interplay of Fiber Nonlinearity and Optical Filtering in Ultra dense WDM," *IEEE, Photon. Technol. Lett.*, vol. 15, pp. 147-149, 2003

[38] Takehiro Tsuritani, Akira Agata, Itsuro Morita, Keiji Tanaka, and Noboru Edagawa, "Performance comparison between DSB and VSB signals in 20Gbit/s-based ultra-long-haul WDM systems," *OFC'2001 Technical Digest*, MM5, 2001

[39] M. R. Phillips, "Distortion by stimulated Brillouin scattering effect in analog video lightwave systems," OFC'97 post deadline paper PD23.

[40] M. R. Phillips, T. E. Darcie, D. Marcuse, G. E. Bodeep, and N. J. Frigo, "Nonlinear distortion generated by dispersive transmission of chirped intensity-modulated signals,' IEEE Photon. Technol.

Lett., vol. 3, pp.481-483, May 1991

[41] Hewlett-Packard Company, "Spectrum analyzer measurement and noise," Application note 1303.

[42] M. C. Wu, P. Y. Chiang and W. I. Way, "On the validity of using CW tones to test the linearity of multiplexed lightwave systems," submitted to Photonics Tech. Letters.

[43] M. R. Phillips, D. W. Anthon, and K. L. Sweeney, "Chromatic dispersion effects in CATV analog lightwave systems using externally modulated transmitters," OFC'96 Post-deadline Paper, PD17-1.

[44] N. S. Bergano and C. R. Davidson, "Circulating Loop Transmission Experiments for the Study of Long-Haul Transmission Systems Using Erbium-Doped Fiber Amplifiers," J. Lightwave Technology, vol.15, pp.879-888, May 1995.

[45] M. C. Wu, C. H. Wang, and W. I. Way, "CSO distortions due to the combined effects of self- and external-phase modulations in long-distance 1550 nm AM-CATV systems," IEEE Photon. Tech. Lett., vol.31, pp.718-720, June 1999.